

# 1 Rethinking the role of transport and photochemistry in regional 2 ozone pollution: Insights from ozone concentration and mass budgets

3 Kun Qu<sup>1,2,3</sup>, Xuesong Wang<sup>1,2</sup>, Xuhui Cai<sup>1,2</sup>, Yu Yan<sup>1,2</sup>, Xipeng Jin<sup>1,2</sup>, Mihalis Vrekoussis<sup>3,4,5</sup>, Maria  
4 Kanakidou<sup>3,6</sup>, Guy Brasseur<sup>7,8</sup>, Jin Shen<sup>9</sup>, Teng Xiao<sup>1,2</sup>, Limin Zeng<sup>1,2</sup>, and Yuanhang Zhang<sup>1,2,10,11</sup>

5 <sup>1</sup>State Key Joint Laboratory of Environmental Simulation and Pollution Control, College of Environmental Sciences and Engineering,  
6 Peking University, Beijing 100871, China

7 <sup>2</sup>International Joint Laboratory for Regional Pollution Control, Ministry of Education, Beijing, 100816, China

8 <sup>3</sup>Laboratory for Modeling and Observation of the Earth System (LAMOS), Institute of Environmental Physics (IUP), University of  
9 Bremen, Bremen, Germany

10 <sup>4</sup>Center of Marine Environmental Sciences (MARUM), University of Bremen, Germany

11 <sup>5</sup>Climate and Atmosphere Research Center (CARE-C), The Cyprus Institute, Cyprus

12 <sup>6</sup>Environmental Chemical Processes Laboratory, Department of Chemistry, University of Crete, Heraklion, Greece

13 <sup>7</sup>Max Planck Institute for Meteorology, Hamburg, Germany

14 <sup>8</sup>National Center for Atmospheric Research, Boulder, Colorado, USA

15 <sup>9</sup>State Key Laboratory of Regional Air Quality Monitoring, Guangdong Key Laboratory of Secondary Air Pollution Research, Guangdong  
16 Environmental Monitoring Center, Guangzhou 510308, China

17 <sup>10</sup>Beijing Innovation Center for Engineering Science and Advanced Technology, Peking University, Beijing 100871, China

18 <sup>11</sup>CAS Center for Excellence in Regional Atmospheric Environment, Chinese Academy of Sciences, Xiamen 361021, China

19 *Correspondence to:* Xuesong Wang (xswang@pku.edu.cn) and Yuanhang Zhang (yhzhang@pku.edu.cn)

20 **Abstract.** Understanding the role of transport and photochemistry is essential to mitigate tropospheric ozone (O<sub>3</sub>) pollution  
21 within a region. In previous studies, the O<sub>3</sub> concentration budget has been widely used to determine the contributions of two  
22 processes to the variations of O<sub>3</sub> concentrations. These studies often conclude that local photochemistry is the main cause of  
23 regional O<sub>3</sub> pollution; however, they fail to explain why O<sub>3</sub> in a targeted region is often primarily derived from O<sub>3</sub> and/or its  
24 precursors transported from the outside regions as reported by many studies of O<sub>3</sub> source apportionment. Here, we present a  
25 method to calculate the hourly contributions of O<sub>3</sub>-related processes to the variations of not only the mean O<sub>3</sub> concentration,  
26 but also the total O<sub>3</sub> mass (the corresponding budgets are noted as the O<sub>3</sub> concentration and mass budget, respectively) within  
27 the atmospheric boundary layer (ABL) of the concerned region. Based on the modelling results of WRF-CMAQ, the two O<sub>3</sub>  
28 budgets were applied to comprehensively understand the effects of transport and photochemistry on the O<sub>3</sub> pollution over the  
29 Pearl River Delta (PRD) region in China. Quantified results demonstrate the different role of transport and photochemistry  
30 when comparing the two O<sub>3</sub> budgets: Photochemistry drives the rapid increase of O<sub>3</sub> concentrations during the day, whereas  
31 transport, especially vertical exchange through the ABL top, controls both rapid O<sub>3</sub> mass increase in the morning and decrease  
32 in the afternoon. The diurnal changes of the transport contributions in the two O<sub>3</sub> budgets highlight the influences of the ABL  
33 diurnal cycle and regional wind fields on regional O<sub>3</sub> pollution. Through high contributions to the O<sub>3</sub> mass increase in the  
34 morning, transport determines that most O<sub>3</sub> in the PRD originates from the global background and emissions outside the region.  
35 However, due to the simultaneous rapid increase of ABL volumes, this process only has a relatively limited effect on O<sub>3</sub>  
36 concentration increase compared to photochemistry, and transport effect on the regional sources of O<sub>3</sub> cannot be illustrated by

37 the O<sub>3</sub> concentration budget. For future studies targeting O<sub>3</sub> and other secondary pollutants with moderately long atmospheric  
38 lifetimes (e.g., fine particulate matter and some of its components), insights from both concentration and mass budgets are  
39 required to fully understand the role of transport, chemistry and other related processes.

## 40 **1 Introduction**

41 Since first recognized as a key contributor to the Los Angeles smog, tropospheric ozone (O<sub>3</sub>) pollution has received  
42 considerable attention in many highly populated areas in the world (Fishman et al., 2003; Schultz et al., 2017; Fleming et al.,  
43 2018; Fowler et al., 2020). Exposure to O<sub>3</sub> threatens crop yields, ecosystems and human health, resulting in increased  
44 mortality and economic losses (Mills et al., 2013; Ainsworth, 2017; Zhang et al., 2019). In addition, O<sub>3</sub> contributes to global  
45 warming not only directly as a greenhouse gas, but also indirectly by damaging plants and suppressing land carbon sinks  
46 (Sitch et al., 2007; Naik et al., 2021). To address these detrimental effects, efforts have been undertaken to reduce O<sub>3</sub> levels  
47 in polluted regions. However, since O<sub>3</sub> is a secondary pollutant produced in the atmosphere by complex non-linear  
48 chemistry, the abatement of O<sub>3</sub> pollution is a challenging task.

49

50 As a prerequisite to effectively control O<sub>3</sub> pollution, firstly, it is imperative to understand the effects of O<sub>3</sub>-related processes  
51 on the abundance of O<sub>3</sub> in the atmosphere. High O<sub>3</sub> concentrations within a region are often attributed to daytime  
52 photochemical production from O<sub>3</sub> precursors, i.e. NO<sub>x</sub> (= NO + NO<sub>2</sub>) and volatile organic compounds (VOCs), under  
53 sunlight. Due to the short lifetime of O<sub>3</sub> precursors (several hours for NO<sub>x</sub> and reactive VOCs (Liu et al., 2016; Seinfeld and  
54 Pandis, 2016; Laughner and Cohen, 2019)), it is generally believed that O<sub>3</sub> photochemistry is mainly linked to the  
55 contributions of local emissions in polluted regions. On the other hand, since O<sub>3</sub> itself has a moderately long atmospheric  
56 lifetime of 20-30 days (Stevenson et al., 2006; Bates and Jacob, 2019), transport processes in the atmosphere, including  
57 horizontal transport (mainly advection) and vertical exchange through the top of the atmospheric boundary layer (ABL), may  
58 also considerably contribute to regional O<sub>3</sub> pollution (Myriokefalitakis et al., 2016). Specifically, through vertical exchange,  
59 O<sub>3</sub> in the residual layer and/or free atmosphere is entrained into the ABL and involved in the ABL mixing after sunrise,  
60 leading to rapidly increasing O<sub>3</sub> concentrations near the surface (Kaser et al., 2017; Hu et al., 2018; Zhao et al., 2019).  
61 Although O<sub>3</sub> produced from local emissions may be transported out and later recirculated back to the region, it is more likely  
62 that transported O<sub>3</sub> is mainly derived from the emissions of O<sub>3</sub> precursors in the upwind regions, continents and even O<sub>3</sub> in  
63 the stratosphere under the combined effect of meso-, synoptic-, large- and global-scale atmospheric movements (Massagué  
64 et al., 2019). If photochemistry has a comparatively large influence on O<sub>3</sub>, reducing local emissions is an appropriate strategy  
65 to alleviate regional O<sub>3</sub> pollution; otherwise, it is necessary to focus on emission control in the upwind regions, aiming to  
66 reduce transport contributions to O<sub>3</sub>.

67

68 In many studies, the O<sub>3</sub> concentration budget was often utilized to quantify the contributions of various transport and  
69 chemical processes to the variations of O<sub>3</sub> concentrations. The changes in the mean O<sub>3</sub> concentration within the ABL ( $\langle c_{O_3} \rangle$ )  
70 can be expressed as the net contributions of all O<sub>3</sub>-related processes (Lenschow et al., 1981; Janssen and Pozzer, 2015; Vilà-  
71 Guerau de Arellano et al., 2015):

$$\frac{\partial \langle c_{O_3} \rangle}{\partial t} = -\bar{u} \frac{\partial \langle c_{O_3} \rangle}{\partial x} - \bar{v} \frac{\partial \langle c_{O_3} \rangle}{\partial y} - \frac{\partial \overline{c_{O_3}' w'}}{\partial z} + S(O_3) \quad (1)$$

72 where  $u$ ,  $v$  and  $w$  refer to wind speeds in the  $x$ -,  $y$ - and  $z$ -direction, respectively. The right side of Eq. (1) describes the  
73 contributions of 1) horizontal transport (advection, the first two terms), 2) vertical exchange through the ABL top  
74 (entrainment and detrainment, the third term), 3) gas-phase chemistry, dry deposition and other processes (the term  $S(O_3)$   
75 indicates their net contributions). The O<sub>3</sub> concentration budget is then derived by integrating these terms over time. It enables  
76 the identification of the processes that produce positive or negative tendencies of the O<sub>3</sub> concentration, and of the processes  
77 that are most influential for regional O<sub>3</sub> pollution. Reported O<sub>3</sub> concentration budgets derived from ground-based  
78 measurements (Su et al., 2018; Tan et al., 2018; Tan et al., 2019; Yu et al., 2020), aircraft-based mobile observations  
79 (Lenschow et al., 1981; Trousdell et al., 2016; Trousdell et al., 2019) and Process Analysis (PA) or similar modules in  
80 chemical transport models (Hou et al., 2014; Li et al., 2021; Yan et al., 2021) in various regions of the globe often suggest  
81 that O<sub>3</sub> production through local photochemistry drives the noon-time increase of O<sub>3</sub> concentration, whereas transport  
82 reduces O<sub>3</sub> concentration over the same period. Conclusively, photochemistry, rather than transport, plays a main role in O<sub>3</sub>  
83 pollution.

84  
85 However, O<sub>3</sub> source apportionment is likely to provide different conclusions about the relative importance of transport and  
86 photochemistry in affecting O<sub>3</sub> pollution. O<sub>3</sub> source apportionment is performed to identify the regional and/or sectoral  
87 origins of O<sub>3</sub>, of which the results are also used to support air pollution control (Clappier et al., 2017; Thunis et al., 2019).  
88 Here, we only discuss the regional origins of O<sub>3</sub>, because the contributions of sources outside the region (or emissions within  
89 the region, defined as local emissions hereafter) provide information on the influence of transport (or photochemistry) on O<sub>3</sub>  
90 pollution. Previous publications often conclude that most O<sub>3</sub> was not derived from local emissions of O<sub>3</sub> precursors, but from  
91 the global background and emissions outside the targeted regions (Guo et al., 2018; Pay et al., 2019; Liu et al., 2020). The  
92 mixing ratios of background O<sub>3</sub> in various regions of the world are mostly within the range of 30-50 ppb (Reid et al., 2008  
93 and references therein), which are sufficiently high to ensure that O<sub>3</sub> originates mainly from non-local sources in less  
94 polluted regions. Since controlling background O<sub>3</sub> is challenging, efforts to control O<sub>3</sub> pollution in polluted regions with high  
95 non-local contributions to O<sub>3</sub> should focus on reducing emissions in upwind regions rather than only local areas (Lelieveld et  
96 al., 2009; Boian and Andrade, 2012; Massagué et al., 2019). One successful example is the establishment of the “Ozone  
97 Transport Region” in the north-eastern United State by the US Environmental Protection Agency, which promotes  
98 collaborative emission reductions among states to address inter-state O<sub>3</sub> transport (Novel, 1992). The above discussion  
99 highlights the importance of transport for regional O<sub>3</sub> pollution, since it often plays a more prominent role than local

100 photochemistry. Apparently, this last statement conflicts with the conclusions derived from the O<sub>3</sub> concentration budget.  
101 Thus, while the O<sub>3</sub> concentration budget is useful for understanding O<sub>3</sub> pollution, it may not completely illustrate the effects  
102 of transport and photochemistry on regional O<sub>3</sub> pollution.

103

104 In the ABL of the concerned region, the mean O<sub>3</sub> concentration and total O<sub>3</sub> mass are both conserved, which means that their  
105 variations are equal to the net contributions by various O<sub>3</sub>-related processes including transport and photochemistry. These  
106 relationships can be represented by the O<sub>3</sub> concentration budget and mass budget, respectively. Unlike the aforementioned  
107 O<sub>3</sub> concentration budget in Eq. (1), the hourly O<sub>3</sub> mass budget, written as

$$\frac{\partial m_{O_3}}{\partial t} = -(\bar{u}s_x\langle c_{O_3} \rangle + \bar{v}s_y\langle c_{O_3} \rangle) - \overline{c_{O_3}'w'}s_z + S(O_3)V \quad (2)$$

108 is seldom reported ( $m_{O_3}$  is the total O<sub>3</sub> mass within the ABL of the region;  $s_x$ ,  $s_y$ ,  $s_z$  are the areas of the interfaces in the x-,  
109 y- and z-direction, respectively;  $V$  is the volume of the ABL column). Due to the varied effects of transport on O<sub>3</sub>  
110 concentration and mass, the O<sub>3</sub> mass budget differs from the O<sub>3</sub> concentration budget but is more suitable to explore the  
111 influence of transport and photochemistry on the results of O<sub>3</sub> source apportionment (more detailed explanations are given in  
112 Sect. 2.4). In order to comprehensively understand the role of transport and photochemistry in regional O<sub>3</sub> pollution, in the  
113 present study, we developed a method to calculate both the O<sub>3</sub> concentration and mass budget based on the simulation results  
114 from the Weather Research and Forecasting (WRF) and Community Multiscale Air Quality (CMAQ) models, and also  
115 analysed, compared the results of the two regional-level O<sub>3</sub> budgets. The Pearl River Delta (PRD) region, a city cluster  
116 located on the southeast coast of China and exposed to severe O<sub>3</sub> pollution in summer and autumn (Gao et al., 2018), was  
117 selected as the targeted region. The tasks for this study can be summarized as follows:

118

#### 119 *1) Development of the method to quantify the two O<sub>3</sub> budgets*

120 WRF-CMAQ employs the Process Analysis (PA) module to assess the contributions of O<sub>3</sub>-related processes to the variations  
121 of O<sub>3</sub> concentrations within each grid cell. However, to obtain the regional-level O<sub>3</sub> concentration and mass budgets, the  
122 results of PA module are not sufficient. One reason is that the contribution of vertical exchange through the ABL top is not  
123 specifically quantified in commonly used ABL parameterizations, thus requires additional calculations (Kaser et al., 2017).  
124 Additionally, calculations based on the PA results are needed to identify the contributions of other O<sub>3</sub>-related processes to  
125 ABL-mean O<sub>3</sub> concentration as well as the results of the O<sub>3</sub> mass budget. To address this, we developed a method to quantify  
126 the two O<sub>3</sub> budgets, of which the details are given in Sect. 2.1-2.3.

127

#### 128 *2) Analysis and comparison of the results from the two O<sub>3</sub> budgets*

129 Based on the simulations of O<sub>3</sub> pollution in the PRD with the model setup introduced in Sect. 2.5, the two O<sub>3</sub> budgets were  
130 calculated for further analyses and comparisons to reveal the role of transport and photochemistry in regional O<sub>3</sub> pollution  
131 from a more comprehensive perspective. Relative discussions are presented in Sect. 3.

132

133 *3) Assessment of the role of transport and photochemistry in determining the regional origins of O<sub>3</sub>*

134 The Brute Force Method (BFM; Clappier et al., 2017), a widely used source apportionment method, was combined with the  
135 O<sub>3</sub> mass budget calculation to determine the contributions of emissions within and outside the PRD as well as background  
136 sources to the O<sub>3</sub> transported into or produced by photochemistry in the region (methodology described in Sect. 2.6). The  
137 results, as discussed in Sect. 4, reveal the impacts of transport and photochemistry in determining the regional origins of O<sub>3</sub>  
138 in the PRD, and explain why the different views on the role of two processes in regional O<sub>3</sub> pollution are suggested by the O<sub>3</sub>  
139 concentration budget and O<sub>3</sub> source apportionment studies.

## 140 **2 Methodology: O<sub>3</sub> budget calculations and model setup**

### 141 **2.1 The PRD grids and O<sub>3</sub>-related processes in O<sub>3</sub> budgets**

142 The two O<sub>3</sub> budgets were calculated for the PRD, of which the grids are shown in the lower-left panel of Fig. 1. These grids  
143 are set based on the finer modelling domain of WRF-CMAQ (details given in Sect. 2.5) and determined according to the  
144 administrative areas of the PRD. The PRD grids with one or several interfaces with the outer regions are defined as the  
145 border grids, and they can be further classified as the grids in the north, south, west and east borders based on their locations.  
146 Correspondingly, the PRD grids with no interface with the outer regions are defined as the non-border grids.

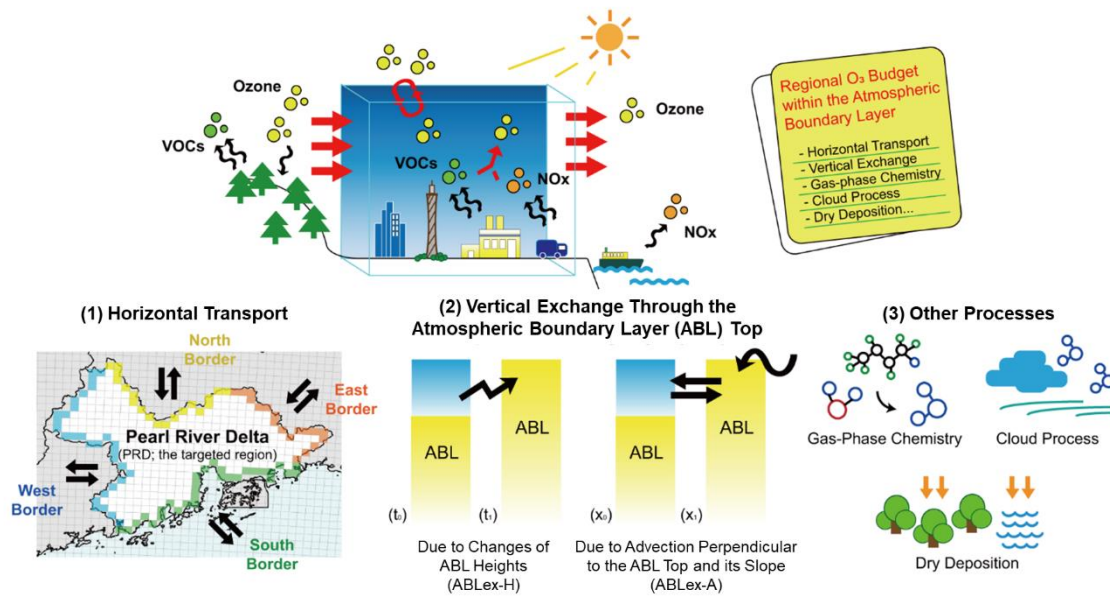
147

148 Figure 1 also displays all O<sub>3</sub>-related processes considered in the calculation of O<sub>3</sub> budgets here. The transport processes  
149 include horizontal transport through the four types of borders and vertical exchange through the ABL top. For vertical  
150 exchange, its contribution in the O<sub>3</sub> concentration budget (the third term on the right side of Eq. (1)) is quantified by (Sinclair  
151 et al., 2010; Jin et al., 2021):

$$-\frac{\partial \overline{c_{O_3}' w'}}{\partial z} = \frac{\Delta c_{O_3}}{H} \frac{\partial H}{\partial t} + \frac{\Delta c_{O_3}}{H} \left( u_h \frac{\partial H}{\partial x} + v_h \frac{\partial H}{\partial y} - w_h \right) \quad (3)$$

152 where  $H$  is the ABL height;  $\Delta c_{O_3}$  is the difference between O<sub>3</sub> concentrations above and within the ABL;  $u_h$ ,  $v_h$  and  $w_h$  are  
153 the ABL-top wind speeds in the x, y and z-direction, respectively. The terms on the right side of Eq. (3) suggest that vertical  
154 exchange through the ABL top, or entrainment and detrainment, is attributed to 1) the temporal changes of ABL heights ( $H$ )  
155 and 2) advection perpendicular to the ABL top and its slope. For the convenience of discussion, hereafter, vertical exchanges  
156 due to the above two dynamic processes are marked as ABLex-H and ABLex-A, respectively. The contributions of all  
157 transport processes in the O<sub>3</sub> budgets were quantified based on meteorological parameters simulated by WRF and O<sub>3</sub>  
158 concentrations simulated by CMAQ. The basic calculations of the contributions from the above-mentioned transport  
159 processes in the O<sub>3</sub> mass and concentration budgets are separately introduced in the following two sections.

160



161

162 **Figure 1.** Schematic illustration of O<sub>3</sub> budgets (the upper panel) and O<sub>3</sub>-related processes considered (the lower panel): (1) Horizontal  
 163 transport through the north, south, west and east borders of the Pearl River Delta (PRD) (the distributions of the PRD grids are also shown:  
 164 yellow, green, blue, orange for the north, south, west and east border grids, respectively, and white for the non-border grids); (2) Vertical  
 165 exchange through the atmospheric boundary layer (ABL) top, including the process due to the changes of ABL heights (ABLex-H) and  
 166 advection perpendicular to the ABL top and its slope (ABLex-A); (3) Other processes, including gas-phase chemistry, cloud process and  
 167 dry deposition for this study.

168

169 Other processes in the O<sub>3</sub> budgets include gas-phase chemistry (including daytime photochemical O<sub>3</sub> production, O<sub>3</sub> titration  
 170 by NO and O<sub>3</sub> depletion with unsaturated VOCs, etc.), cloud process (including below and in-cloud mixing, aqueous-phase  
 171 chemistry, wet deposition; Liu et al., 2011) and dry deposition. The contributions of these processes are all calculated based  
 172 on the output of the PA module in CMAQ. In a word, their contributions in the O<sub>3</sub> mass budget are obtained by summing up  
 173 the contributions in all grid cells within the ABL of the PRD, and their contributions in the O<sub>3</sub> concentration budget are the  
 174 corresponding contributions to O<sub>3</sub> mass divided by the volume of the ABL of the PRD. Since diffusion through the side and  
 175 top boundaries of the region is expected to have a negligible influence on the variations of both O<sub>3</sub> concentration and mass,  
 176 we did not consider this process in O<sub>3</sub> budget calculations.

177

178 The calculation process of the two O<sub>3</sub> budgets is summarized as follows. Based on multiple output files of WRF and CMAQ,  
 179 firstly, the contributions of all considered O<sub>3</sub>-related processes to O<sub>3</sub> mass changes and volumes/volume changes linked to  
 180 these processes within the ABL are calculated in nearly all grids of the modelling domain. We developed the post-processing  
 181 tool *flux\_4d\_cal* to conduct the above calculations. Afterwards, the regional-level O<sub>3</sub> mass and concentration budgets are  
 182 quantified based on the results of the first-step calculations. Particularly, the method described in Sect. 2.3 is applied to

183 estimate the contributions of O<sub>3</sub>-related processes in the O<sub>3</sub> concentration budget. More detailed descriptions of the  
 184 calculation process can be found in Text S1.

## 185 2.2 Transport contributions in the O<sub>3</sub> mass budget

186 The method by Yang et al. (2012) and Chang et al. (2018) was applied to quantify the contributions of horizontal transport in  
 187 the O<sub>3</sub> mass budget. For instance, the contribution of the advection through the west/east interface of a grid column within  
 188 the ABL to total O<sub>3</sub> mass ( $F_{htrans}$ ) in the column during the time interval  $dt$  is calculated as:

$$F_{htrans} = \int_0^H c_{O_3} u L dz dt \quad (4)$$

189 where  $L$  is the width of the grid (equal to the horizontal resolution in the model);  $dz$  is the height of vertical layers. For  
 190 advection through the north/south interface, the calculation is similar to Eq. (4), except for using  $v$  instead of  $u$ .  $F_{htrans}$   
 191 values through all interfaces between the border grids and the outer region were calculated. Afterwards, they are summed up  
 192 separately according to the types of borders as the net contributions of horizontal transport through the north, south, west and  
 193 east borders of the PRD in the O<sub>3</sub> mass budget.

194

195 Following Sinclair et al. (2010) and Jin et al. (2021), the contribution of vertical exchange through the ABL top to O<sub>3</sub> mass  
 196 ( $F_{ABLex}$ ) during the time interval  $dt$  can be expressed as:

$$F_{ABLex} = F_{ABLex-H} + F_{ABLex-A} = c_{O_3,h} \frac{\partial H}{\partial t} L^2 dt + c_{O_3,h} \left( u_h \frac{\partial H}{\partial x} + v_h \frac{\partial H}{\partial y} - w_h \right) L^2 dt \quad (5)$$

197 where  $c_{O_3,h}$  is the O<sub>3</sub> concentration at the ABL top. The two terms on the right-most side of Eq. (5) separately describe the  
 198 contributions of ABLex-H and ABLex-A (denoted separately as  $F_{ABLex-H}$  and  $F_{ABLex-A}$ ).  $F_{ABLex}$  values in all the grids over  
 199 the PRD were summed up to derive the net contribution of vertical exchange through the ABL top in the O<sub>3</sub> mass budget.

## 200 2.3 Transport contributions in the O<sub>3</sub> concentration budget

201 It is difficult to directly apply Eq. (1) in the quantification of transport contributions in the regional-level O<sub>3</sub> concentration  
 202 budget. Therefore, a different approach was applied, which is introduced as follows.

203

204 Suppose that an air parcel with a total volume of  $dV$  is transported into the ABL of the PRD (its original volume is  $V$ ). The  
 205 variation of  $\langle c_{O_3} \rangle$  under the influence of horizontal transport ( $d\langle c_{O_3} \rangle_{htrans}$ ) can be written as:

$$d\langle c_{O_3} \rangle_{htrans} = \frac{F_{htrans} + \langle c_{O_3} \rangle (V - dV)}{V} - \langle c_{O_3} \rangle = \frac{F_{htrans} - \langle c_{O_3} \rangle dV}{V} \quad (6)$$

206 Since ABLex-A is also an advection process, its contribution in the O<sub>3</sub> concentration budget ( $d\langle c_{O_3} \rangle_{ABLex-A}$ ) can be  
 207 quantified using a similar formula as Eq. (6), except for using  $F_{ABLex-A}$  instead of  $F_{htrans}$ .

208

209 Through ABLex-H, air parcels in the residual layer and/or free atmosphere are merged into the ABL or vice versa. Thus, the  
 210 variation of  $\langle c_{O_3} \rangle$  under its influence ( $d\langle c_{O_3} \rangle_{ABLex-H}$ ) is expressed as:

$$d\langle c_{O_3} \rangle_{ABLex-H} = \frac{F_{ABLex-H} + \langle c_{O_3} \rangle V}{V + dV} - \langle c_{O_3} \rangle = \frac{F_{ABLex-H} - \langle c_{O_3} \rangle dV}{V + dV} \quad (7)$$

211

212 If the targeted region is small enough, the expressions of  $d\langle c_{O_3} \rangle_{htrans}$  and  $d\langle c_{O_3} \rangle_{ABLex-H}$  in Eqs. (6) and (7) can be  
 213 transformed to the corresponding terms in Eq. (1), confirming the applicability of the above calculations (for details, see  
 214 Text S2). All variables in Eqs. (6) and (7) can be quantified by the post-processing tool *flux\_4d\_cal*, making the method  
 215 feasible and suitable for the afterward calculations of the regional-scale O<sub>3</sub> concentration budget.

216

217 However, due to the prominent diurnal cycle of ABL,  $V$  in Eqs. (6) and (7) may change notably within an hour, leading to  
 218 bias in the hourly estimations of  $d\langle c_{O_3} \rangle_{htrans}$ ,  $d\langle c_{O_3} \rangle_{ABLex-H}$  and  $d\langle c_{O_3} \rangle_{ABLex-A}$  when using  $V$  at the start and end of the  
 219 hour. This problem also applies to the calculation of contributions from other O<sub>3</sub>-related processes. In order to reduce the  
 220 potential bias caused by the different selections of  $V$ , we designed two calculation paths for the hourly O<sub>3</sub> concentration  
 221 budget (Fig. S1):

- 222 • O<sub>3</sub> mass change → ABL volume change
- 223 • ABL volume change → O<sub>3</sub> mass change

224 where only O<sub>3</sub> mass or ABL volume changes in each calculation step. The contribution of ABLex-H to O<sub>3</sub> concentration can  
 225 be viewed as the net effects of ABL volume change and O<sub>3</sub> being transported into/out of the ABL: ABL volume change due  
 226 to ABL development (collapse) leads to lower (higher) O<sub>3</sub> concentration, and O<sub>3</sub> transported into (out of) the ABL through  
 227 ABLex-H leads to O<sub>3</sub> increase (decrease). These contributions are quantified separately in the ABL volume and O<sub>3</sub> mass  
 228 change step. The contributions of horizontal transport, ABLex-A and non-transport processes are quantified only in the O<sub>3</sub>  
 229 mass change step. The contribution of each process to the variation of O<sub>3</sub> concentration is calculated using both paths, and  
 230 the mean value of two results serves as an estimation close to its real contribution in the O<sub>3</sub> concentration budget.

## 231 2.4 Difference between the two O<sub>3</sub> budgets

232 The difference between the two O<sub>3</sub> budgets is linked to the varied effect of transport on O<sub>3</sub> mass and concentration. Suppose  
 233 that the mean O<sub>3</sub> concentration in the transported air parcels is  $\langle c_{O_3} \rangle_{trans}$ . For horizontal transport, its contributions in the O<sub>3</sub>  
 234 mass and concentration budgets can be separately written as:

$$F_{htrans} = \langle c_{O_3} \rangle_{trans} dV \quad (8)$$

$$d\langle c_{O_3} \rangle_{htrans} = \frac{dV}{V} (\langle c_{O_3} \rangle_{trans} - \langle c_{O_3} \rangle) \quad (9)$$

235 Apparently,  $F_{htrans}$  is related to the O<sub>3</sub> concentrations in the transported air parcels, but not to those in the studied region. It  
 236 indicates the amount of O<sub>3</sub> mass transported into or out of the region. Whether it is positive or negative only depends on the



237 direction of transport — O<sub>3</sub> being transported into (out of) the region leads to the increase (decrease) of O<sub>3</sub> mass, which  
 238 corresponds to a positive (negative) contribution in the O<sub>3</sub> mass budget. In contrast,  $d\langle c_{O_3} \rangle_{htrans}$  quantifies how much  
 239 horizontal transport alters regional-mean O<sub>3</sub> concentrations, and is linked to the difference between O<sub>3</sub> concentrations in the  
 240 transported air parcels and the studied region (Eq. (9)). O<sub>3</sub> being transported into (out of) the region does not necessarily  
 241 result in a higher (lower) O<sub>3</sub> concentration. For instance, when clean air parcels with relatively low O<sub>3</sub> levels are transported  
 242 into the region, they dilute O<sub>3</sub> pollution and reduce O<sub>3</sub> concentration ( $d\langle c_{O_3} \rangle_{htrans} < 0$ ). Given that ABLex-A is also an  
 243 advection process, the above difference also applies to this process. For ABLex-H, its contributions in the O<sub>3</sub> mass and  
 244 concentration budgets are expressed as:

$$F_{ABLex-H} = \langle c_{O_3} \rangle_{trans} dV \quad (10)$$

$$d\langle c_{O_3} \rangle_{ABLex-H} = \frac{dV}{V + dV} (\langle c_{O_3} \rangle_{trans} - \langle c_{O_3} \rangle) \quad (11)$$

245 Similarly, ABL development and collapse lead to the increase and decrease of O<sub>3</sub> mass, respectively, but whether they  
 246 contribute to higher or lower O<sub>3</sub> concentration also depends on the difference between O<sub>3</sub> concentration in the transported air  
 247 parcels and that in the region. Based on the above discussion, these transport processes all show different effects on O<sub>3</sub> mass  
 248 and concentration — the effect of transport on the variations of O<sub>3</sub> mass is only related to the characteristics of the  
 249 transported air parcels, namely their volumes and O<sub>3</sub> concentrations within (Eqs. (8) and (10)), while how transport  
 250 contributes to the variations of O<sub>3</sub> concentration is linked to the difference between O<sub>3</sub> concentrations in the transported air  
 251 parcels and the region (Eqs. (9) and (11)).

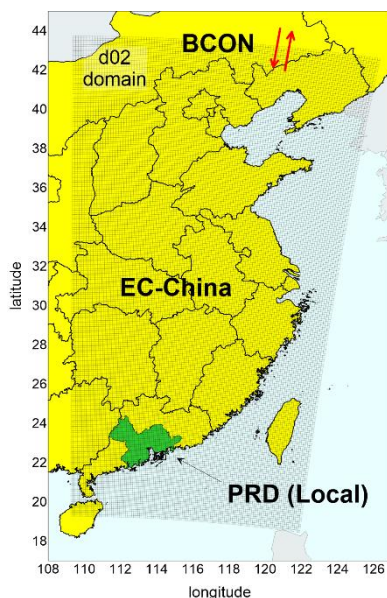
252

253 To properly analyse the impact of transport and photochemistry on the regional origins of O<sub>3</sub>, it is required to identify the  
 254 regional origins of the “new O<sub>3</sub>” into the studied region and the “disappeared O<sub>3</sub>” out of the studied region contributed by  
 255 various O<sub>3</sub>-related processes, rather than how these processes lead to the variations of O<sub>3</sub> concentration. Thus, the influence  
 256 of transport and photochemistry on the results of O<sub>3</sub> source apportionment can be explored by the O<sub>3</sub> mass budget, but not by  
 257 the O<sub>3</sub> concentration budget. By utilizing the BFM source apportionment method in combination with the O<sub>3</sub> mass budget  
 258 calculation, we can identify the regional origins of O<sub>3</sub> mass increase and decrease due to transport and photochemistry, and  
 259 explain how these processes determine the results of O<sub>3</sub> source apportionment in the PRD.

## 260 **2.5 Model setup and validation**

261 The O<sub>3</sub> concentration and mass budgets within the ABL of the PRD were calculated based on the WRF-CMAQ modelling  
 262 results by Qu et al. (2021a). The WRF (version 3.2) and CMAQ (version 5.0.2) models were used to simulate the  
 263 meteorological and pollutant fields, respectively. Two domains with the resolution of 36 and 12 km (denoted as d01 and d02  
 264 hereafter) were set up for the one-way nested simulations, and the results in the finer d02, which includes the PRD and most  
 265 areas in East and Central China (Fig. 2), were used in the calculations of O<sub>3</sub> budgets. To represent the contributions of global  
 266 background to O<sub>3</sub>, the initial and boundary conditions for the coarse d01 domain were provided from the global model, the

267 Model for Ozone and Related Chemical Tracers, version 4 (MOZART-4). The PRD inventory provided by the Guangdong  
268 Environmental Monitoring Centre, the Multi-resolution Emission Inventory for China (MEIC) inventory for the mainland  
269 China (He, 2012), the MIX inventory for the Asian regions outside of mainland China (Li et al., 2017) and biogenic  
270 emissions simulated by the Model of Emissions of Gases and Aerosols from Nature (MEGAN; version 2.10) model were  
271 used in the simulations. SAPRC07 (Carter, 2010) and AERO6 were applied as the gas-phase chemistry mechanism and the  
272 aerosol scheme, respectively. The simulations of O<sub>3</sub> pollution in the PRD were performed for October 2015 (October 11–  
273 November 10, 2015) and July 2016 (July 1–31, 2016), which serve as the representative months in autumn and summer,  
274 respectively. Here, O<sub>3</sub> polluted days are defined when the maximum hourly O<sub>3</sub> concentrations of the day exceed 200 µg/m<sup>3</sup>,  
275 or the maximum 8-hour average O<sub>3</sub> concentrations of the day exceed 160 µg/m<sup>3</sup> (both are the Grade-II O<sub>3</sub> thresholds in the  
276 Chinese National Ambient Air Quality Standard) in any municipality of the PRD. According to this definition, there were 16  
277 and 12 O<sub>3</sub> polluted days in the two months, respectively (more information is given in Table S1). The mean O<sub>3</sub> budgets  
278 during these O<sub>3</sub> polluted days of two seasons were separately calculated and discussed in the present study.



279  
280 **Figure 2.** The spatial distributions of the d02 modelling domain and source regions. The d02 domain is displayed as the nested areas in the  
281 figure. PRD, Pearl River Delta; EC-China, East and Central China; BCON, the boundary conditions of d02 modelling, or the contributions  
282 of sources outside the d02 domain.  
283

284 We evaluated the performance of WRF-CMAQ modelling based on multiple observational datasets. The modelling results of  
285 meteorological parameters (including temperature, relative humidity and wind speed), O<sub>3</sub>, NO<sub>2</sub> concentrations and the  
286 mixing ratios of hydrocarbons were validated with corresponding observations in the PRD by Qu et al. (2021a). The  
287 performance of the model in simulating the above variables was overall satisfying with low biases and high correlations (for  
288 details, see Qu et al., 2021a). In this study, we further compared the modelled ABL height, the vertical profiles of wind  
289 speed, direction and O<sub>3</sub> mixing ratio in Hong Kong (located in the south PRD) with corresponding observations from the

290 IAGOS (In-service Aircraft for a Global Observing System; Petzold et al., 2015) dataset. The modelled ABL heights showed  
 291 similar hourly variations during the day as the observational results ( $R = 0.76$ ), with a mean bias of  $-1.1$  m (Fig. S2). The  
 292 mean biases of mean wind speeds are within the range of  $\pm 1$  m/s in all considered height ranges (0-1 km, 1-2 km, 2-5 km),  
 293 and the results of the IAGOS and WRF model indicate similar variations of prevailing wind directions in different seasons  
 294 and height ranges (Fig. S3). Moreover, modelled  $O_3$  mixing ratios in Oct. 2015 are overestimated by 6% and 26% in the  
 295 height range of 0-1 km and 1-2 km, respectively, and sufficiently illustrate the development, maintenance and dissipation of  
 296  $O_3$  pollution during the month (Fig. S4). More detailed evaluations on the model performance of these parameters are  
 297 presented in Text S3 of the Supplement. Overall, the model performance is acceptable, indicating that the model can provide  
 298 reasonable data for the calculations of  $O_3$  budgets.

299

300 If the calculation methods and assumptions are reasonable, the conservation of  $O_3$  concentration and mass budgets, described  
 301 as

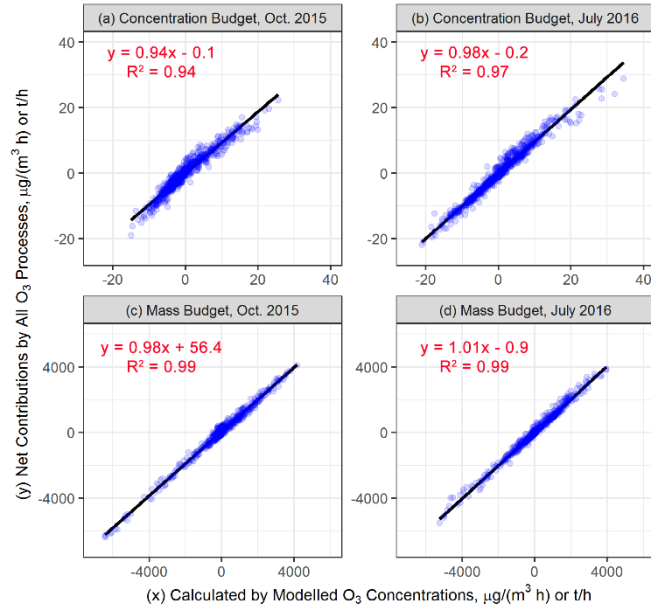
$$\frac{\partial \langle c_{O_3} \rangle (or\ m_{O_3})}{\partial t} - (S_{htrans} + S_{ABLex} + S_{chem} + S_{cloud} + S_{ddep}) = 0 \quad (12)$$

302 can be achieved (the terms  $S_{htrans}$ ,  $S_{ABLex}$ ,  $S_{chem}$ ,  $S_{cloud}$  and  $S_{ddep}$  indicate the contributions of horizontal transport, vertical  
 303 exchange through the ABL top, gas-phase chemistry, cloud process and dry deposition, respectively, in the  $O_3$  concentration  
 304 or mass budgets). Therefore, we used Eq. (12) to examine the validity of  $O_3$  budget calculations. Total  $O_3$  masses at the start  
 305 and end of each hour were directly used to calculate the hourly variations of  $O_3$  mass ( $\frac{\partial m_{O_3}}{\partial t}$ ). Besides these two parameters,  
 306 the volumes of the ABL of the PRD at the start and end of each corresponding hour (calculated using ABL heights in all the  
 307 PRD grids) are also needed to calculate the hourly variations of  $O_3$  concentration ( $\frac{\partial \langle c_{O_3} \rangle}{\partial t}$ ). The contributions of various  $O_3$ -  
 308 related processes in the  $O_3$  concentration and mass budgets were quantified using the method introduced in Sect. 2.1-2.3. As  
 309 displayed in Fig. 3, hourly variations of  $O_3$  concentration/mass and the corresponding net contributions from all  $O_3$ -related  
 310 processes show good correlations ( $R^2 > 0.9$ ), with all fitted lines close to the 1:1 line. Thus, the conservation is overall met  
 311 for the two  $O_3$  budgets in both representative months, allowing for further analyses based on the quantified budgets.

## 312 **2.6 Identifying regional origins of $O_3$ mass changes due to transport and photochemistry**

313 The question to be addressed is how  $O_3$ -related processes determine the regional origins of  $O_3$ . By combining the  $O_3$  mass  
 314 budget calculations with the BFM source apportionment method, we identified the regional origins of  $O_3$  mass changes due  
 315 to transport and photochemistry (gas-phase chemistry). Here, the interest lies in the contributions of emissions in the PRD  
 316 (also defined as local emissions), in other regions within d02 (mainly East and Central China, hereafter denoted as EC-  
 317 China), and in regions outside the d02 (the boundary conditions (BCON) of d02 modelling; representative of the background  
 318 sources). The distribution of these source regions is shown in Fig. 2. Besides the base scenario where all emissions in d02  
 319 were considered in simulations, three sensitivity scenarios were additionally simulated:

- 320 • The PRD\_zero scenario: All emissions (including anthropogenic and biogenic emissions; the same below) in the  
 321 PRD were zeroed out;
- 322 • The EC-China\_zero scenario: All emissions in the EC-China were zeroed out;
- 323 • The All\_zero scenario: All emissions within d02 were shut down.



324  
 325 **Figure 3.** The examinations of O<sub>3</sub> budget conservation in Oct. 2015 (a,c) and July 2016 (b,d) for the hourly O<sub>3</sub> concentration budget (a-b)  
 326 and mass budget (c-d). The units for the O<sub>3</sub> concentration and mass budgets are µg/(m<sup>3</sup> h) and t/h, respectively. The solid black lines in the  
 327 plots are the fitted lines.

328 The hourly contributions of the process  $i$  in the O<sub>3</sub> mass budget were quantified using the same method outlined in Sect. 2.1-  
 329 2.2 for the base scenario and three sensitivity scenarios, denoted as  $f_{i,base}$ ,  $f_{i,PRD\_zero}$ ,  $f_{i,EC-China\_zero}$ , and  $f_{i,all\_zero}$ ,  
 330 respectively. These parameters enable the determination of the contributions of emissions from the PRD and EC-China as  
 331 well as the background sources (BCON) to the O<sub>3</sub> mass increase and decrease due to various O<sub>3</sub>-related processes. The  
 332 contributions of BCON in the O<sub>3</sub> mass changes due to the process  $i$  ( $F_{i,BCON}$ ) can be estimated directly as the contributions of  
 333 the process  $i$  to the O<sub>3</sub> mass in the All\_zero scenario:

$$F_{i,BCON} = f_{i,all\_zero} \quad (13)$$

334 For the contributions of the PRD and EC-China emissions from the process  $i$  (separately denoted as  $F_{i,PRD}$  and  $F_{i,EC-China}$ ),  
 335 they can be derived in two ways: 1) by subtracting simulations with zeroed studied emissions from the base case simulation  
 336 (top-down BFM); 2) by subtracting simulations without all emissions from simulations accounting only for studied  
 337 emissions (bottom-up BFM). Due to the non-linear response of O<sub>3</sub> to precursor emissions, the results from top-down and  
 338 bottom-up BFM can differ, which may lead to the non-additivity of the results (the sum of all contributions is not equal to

339 the concerned metric; here,  $F_{i,PRD} + F_{i,EC-China} + F_{i,BCON} \neq f_{i,base}$ ). Therefore, we estimated  $F_{i,PRD}$  and  $F_{i,EC-China}$  as the  
340 average values of the contributions by using top-down BFM and bottom-up BFM:

$$F_{i,PRD} = \frac{1}{2} [(f_{i,base} - f_{i,PRD\_zero}) + (f_{i,EC-China\_zero} - f_{i,all\_zero})] \quad (14)$$

$$F_{i,EC-China} = \frac{1}{2} [(f_{i,base} - f_{i,EC-China\_zero}) + (f_{i,PRD\_zero} - f_{i,all\_zero})] \quad (15)$$

341 It should be noted that to identify the origins of both “new O<sub>3</sub>” into the region and “disappeared O<sub>3</sub>” out of the region, the  
342 positive and negative contributions of O<sub>3</sub>-related processes to the O<sub>3</sub> mass in the PRD grids were separately summed up for  
343 the base and sensitivity scenarios and quantified using Eqs. (13-15).

### 344 3 Analyses and comparisons of O<sub>3</sub> concentration and mass budget

#### 345 3.1 O<sub>3</sub> concentration budget

346 The upper panels of Fig. 4 show the mean diurnal changes of the O<sub>3</sub> concentration budget within the ABL of the PRD.  
347 According to the net contributions from all O<sub>3</sub>-related processes considered, ABL-mean O<sub>3</sub> concentration increased during  
348 most hours in the daytime, with the highest rates occurring in the early morning (8:00-10:00 local time (LT) in autumn, 7:00-  
349 9:00 LT in summer). The reduction of ABL-mean O<sub>3</sub> concentration in the late afternoon and at night was also considerable.  
350 Its rate reached the maximum value near the sunset time (~18:00 LT in autumn, ~19:00 LT in summer) and gradually  
351 decreased throughout the night. The following question is then raised on the suitability of the budget targeting on ABL-mean  
352 O<sub>3</sub> concentration to explain the variations of O<sub>3</sub> concentrations near the ground. To answer this question, we compared the  
353 hourly changes of modelled ABL-mean O<sub>3</sub> concentration with those of observed and modelled mean near-surface O<sub>3</sub>  
354 concentrations in 18 sites of the Guangdong-Hong Kong-Macao PRD Regional Air Quality Monitoring Network  
355 (distributions shown in Fig. S5). As presented in Fig. S6, these datasets display similar patterns of O<sub>3</sub> diurnal changes. Since  
356 O<sub>3</sub> was well mixed within the ABL (Fig. S4), especially during daytime when O<sub>3</sub> levels are higher than those at night, the  
357 budget of ABL-mean O<sub>3</sub> concentration can reveal the influences of transport and photochemistry on the variations of overall  
358 O<sub>3</sub> levels as well as the causes of O<sub>3</sub> pollution in the targeted region.

359

360 Next, the contributions of various O<sub>3</sub>-related processes in the O<sub>3</sub> concentration budget are discussed as follows:

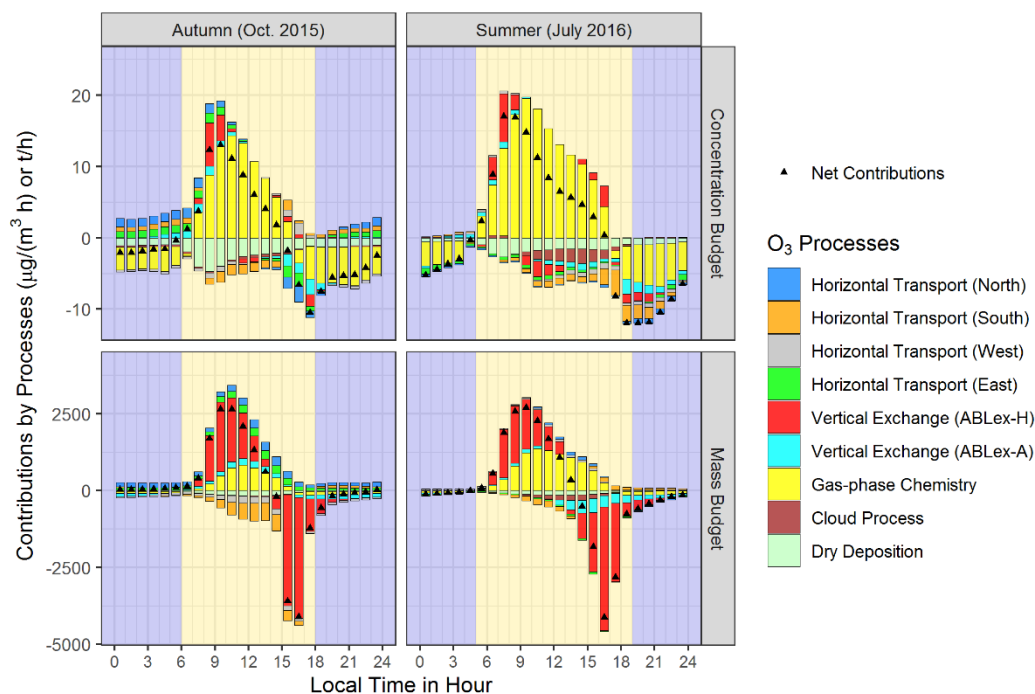
- 361 • Gas-phase chemistry: Figure 4 shows that gas-phase chemistry controlled almost exclusively the O<sub>3</sub> concentration  
362 budget. During the morning hours, which are defined as the period from sunrise (~6:00 LT in autumn, ~5:00 LT in  
363 summer) to the O<sub>3</sub>-peak hour (~14:00 LT), gas-phase chemistry (photochemistry) contributed to, on average, 74%  
364 and 95% of the O<sub>3</sub> concentration increase in autumn and summer, respectively. These contributions are notably  
365 higher than the contributions of transport in the same periods (25% in autumn, 5% in summer). In the afternoon,  
366 gas-phase chemistry was still the main process to maintain high O<sub>3</sub> concentrations within the PRD, but its

367 contributions gradually decreased. However, this process led to decreased O<sub>3</sub> concentration at night, suggesting the  
368 impact of O<sub>3</sub> titration by emitted NO and O<sub>3</sub> depletion with unsaturated VOCs. It may also be related to the  
369 production of particle nitrate through N<sub>2</sub>O<sub>5</sub> hydrolysis (Qu et al., 2021b).

- 370 • Transport: The dominance of gas-phase chemistry in the O<sub>3</sub> concentration budget does not mean that the influence  
371 of transport on O<sub>3</sub> concentration can be neglected all day long. Considerable contributions of transport (mainly by  
372 ABLex-H) to O<sub>3</sub> concentration increase are found during 2-3 hours after sunrise, with the highest hourly mean  
373 contributions reaching ~40% and ~25% in autumn and summer, respectively. This result indicates the notable  
374 influence of air masses with high O<sub>3</sub> concentrations being entrained from residual layers on near-surface O<sub>3</sub>  
375 pollution. ABLex-A and horizontal transport may contribute to the increase or decrease of ABL-mean O<sub>3</sub>  
376 concentration, depending on the O<sub>3</sub> levels in air parcels transported into and out of the region (further analysis is  
377 provided in Sect. 3.3). Overall, these two transport processes had only limited contributions to the variations of O<sub>3</sub>  
378 concentration.
- 379 • Other processes: Dry deposition contributed to a considerable decrease in O<sub>3</sub> concentration, especially during  
380 daytime, and thus served as an important sink process for near-surface O<sub>3</sub>. Besides, cloud process was also an  
381 important sink process for O<sub>3</sub> in summer, which might be related to the convective vertical transport of O<sub>3</sub>.

382  
383 In summary, the results of the O<sub>3</sub> concentration budget indicate that gas-phase chemistry played a major role in the variations  
384 of O<sub>3</sub> concentrations in the PRD. In particular, photochemistry led to the rapid formation of O<sub>3</sub> pollution during daytime,  
385 rather than transport. Our conclusions agree well with those in earlier studies on the O<sub>3</sub> concentration budget (Lenschow et  
386 al., 1981; Hou et al., 2014; Trousdell et al., 2016; Su et al., 2018; Tan et al., 2018; Tan et al., 2019; Trousdell et al., 2019; Yu  
387 et al., 2020; Li et al., 2021; Yan et al., 2021).

388



389

390 **Figure 4.** Mean diurnal changes of the O<sub>3</sub> concentration budget (upper panels) and mass budget (lower panels) on the polluted days of  
 391 representative months in autumn (Oct. 2015; left panels) and summer (July 2016; right panels) within the atmospheric boundary layer of  
 392 the Pearl River Delta. The units for the O<sub>3</sub> concentration and mass budgets are  $\mu\text{g}/(\text{m}^3 \text{ h})$  and  $\text{t}/\text{h}$ , respectively. Backgrounds in yellow and  
 393 dark blue indicate daytime and nighttime periods, respectively.

### 394 3.2 O<sub>3</sub> mass budget

395 The results of the O<sub>3</sub> mass budget are displayed in the lower panels of Fig. 4. The total O<sub>3</sub> mass within the ABL of the PRD  
 396 increased during the morning hours, decreased rapidly in the afternoon and slowly at the early night, then remained stable  
 397 until sunrise in both seasons. The change of total O<sub>3</sub> mass agrees well with the ABL diurnal cycle (Lee, 2018) — daytime  
 398 ABL development (or collapse) and notable O<sub>3</sub> mass increase (or decrease) almost occurred simultaneously, and the  
 399 negligible changes in O<sub>3</sub> mass during most hours of the night may be linked to the small variations of stable ABL.

400

401 We analysed the contributions of various O<sub>3</sub>-related processes in the O<sub>3</sub> mass budget as well, presented as follows:

- 402 • Transport: Unlike the results of the O<sub>3</sub> concentration budget, transport plays a prominent role in the O<sub>3</sub> mass budget.  
 403 On average, it contributed 78% and 53% to O<sub>3</sub> mass increase during the morning hours of autumn and summer,  
 404 respectively, and over 90% to O<sub>3</sub> mass decrease during the afternoon hours of both seasons (14:00-18:00 LT in  
 405 autumn and 14:00-19:00 LT in summer). Most O<sub>3</sub> was transported into or out of the PRD by vertical exchange  
 406 through the ABL top, especially ABLex-H, which links the diurnal changes of O<sub>3</sub> mass and ABL. That is to say,  
 407 when the height of ABL rise (drop) rapidly, a big amount of O<sub>3</sub> is transported into (out of) the ABL through the  
 408 ABLex-H. The contributions of ABLex-A and horizontal transport to O<sub>3</sub> mass change were relatively limited.

409 However, they indicate well the characteristics and variations of regional wind fields in the PRD (more details are  
410 provided in the next section).

- 411 • Gas-phase chemistry: Gas-phase chemistry (photochemistry) also contributed to the increasing O<sub>3</sub> mass in the  
412 daytime, especially in summer. However, its mean contributions during the morning hours (22% in autumn, 47% in  
413 summer) were lower than those of transport.
- 414 • Other processes: Dry deposition and cloud process both acted as O<sub>3</sub> sink processes, but with negligible  
415 contributions to O<sub>3</sub> mass.

416

417 Based on the above discussions, transport tends to be more important than photochemistry in the O<sub>3</sub> mass budget, which  
418 differs from the conclusions of the O<sub>3</sub> concentration budget. The main role of transport, especially ABLex-H, in the O<sub>3</sub> mass  
419 budget suggests the marked impacts of the ABL diurnal cycle on regional O<sub>3</sub> pollution. Despite of less notable influence of  
420 transport on O<sub>3</sub> concentration increase in comparison to that of photochemistry, massive O<sub>3</sub> being transported into the ABL  
421 of the targeted region during the morning hours nearly determines the regional origins of O<sub>3</sub> pollution. Quantified results  
422 combining the O<sub>3</sub> mass budget and source apportionment are further discussed in Sect. 4.

### 423 **3.3 Influences of regional wind fields on O<sub>3</sub> pollution: more analyses of transport contributions in O<sub>3</sub> budgets**

424 As discussed before, the contributions of horizontal transport and ABLex-A were relatively limited in the two O<sub>3</sub> budgets.  
425 However, they illustrate well the influences of regional wind fields, including the seasonal prevailing winds and local  
426 circulations (sea breezes), on O<sub>3</sub> pollution in the PRD. Two main findings from the analyses of these transport contributions  
427 are presented below.

#### 428 **3.3.1 Transport contributions in autumn: The characteristics of prevailing winds**

429 In the PRD, northerly and easterly winds prevail in autumn (as indicated by the wind roses in Fig. S3). Correspondingly, O<sub>3</sub>  
430 was transported into the PRD through its north and east borders, out of the PRD through the south and west borders, as  
431 indicated by the O<sub>3</sub> mass budget (Fig. 4). O<sub>3</sub> masses transported out of the PRD were generally higher than those transported  
432 into the PRD during daytime. This is attributed to higher O<sub>3</sub> concentrations in the downwind regions due to O<sub>3</sub> production  
433 mostly from local emissions. “Low O<sub>3</sub> in, high O<sub>3</sub> out” also explains why horizontal transport led to the net decrease of O<sub>3</sub>  
434 concentration during daytime. At night, O<sub>3</sub> was still transported into the region through the north and east borders of the  
435 PRD, but these processes contributed to the increase of O<sub>3</sub> concentrations. That is to say, with relatively higher O<sub>3</sub>  
436 concentrations compared to those in the NO<sub>x</sub>-titrated urban atmosphere, air parcels transported from the upwind outskirts  
437 served as the supply to slowdown night-time O<sub>3</sub> level decrease in the PRD due to chemistry and deposition.

438

439 The daytime contributions of ABLex-A in the O<sub>3</sub> mass budget also indicate the effects of prevailing northerly winds. The  
440 PRD has mountainous regions in the northern, western and eastern outskirts, as well as urban regions with lower altitudes in



441 the central plain (Fig. S5). As shown in Fig. S7a-b, the positive contributions of ABLex-A through the ABL top (in the z-  
442 direction) can be found in the mountainous northern PRD, suggesting that northerly winds resulted in the downward  
443 transport of O<sub>3</sub> along the terrain. Daytime ABL heights in urban regions were, in general, higher than those in the  
444 surrounding mountainous regions, which is the other reason why O<sub>3</sub> can be transported through the ABL slope (in the x-/y-  
445 direction) near the urban-rural interfaces when northerly wind prevailed (Fig. S7c-d). For the O<sub>3</sub> concentration budget,  
446 ABLex-A contributed to increased O<sub>3</sub> concentration during several hours after sunrise but decreased O<sub>3</sub> concentration in the  
447 afternoon. This different effect is attributed to different comparison results between ABL and above-ABL mean O<sub>3</sub>  
448 concentrations in the two periods (O<sub>3</sub> concentration above the ABL is overall higher than that within the ABL in the  
449 morning, while the opposite is for the afternoon; Fig. S4).

450

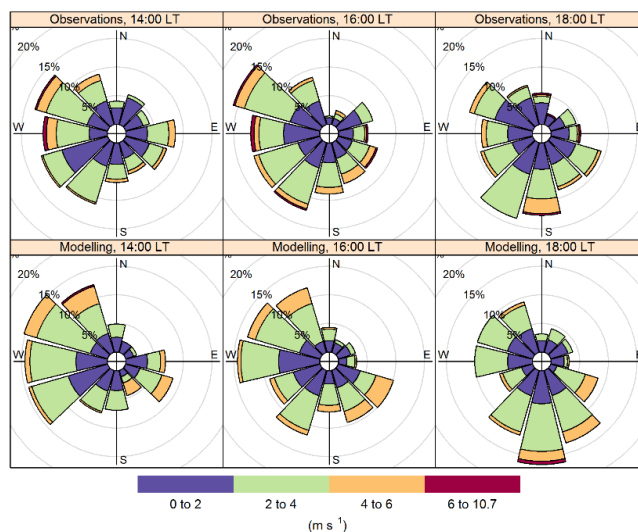
### 451 **3.3.2 Transport contributions in summer: The influence of sea breezes**

452 Although southerly winds normally prevail in summer in the PRD (Fig. S3), on O<sub>3</sub> polluted days, air parcels from other  
453 directions could also influence the region (Qu et al., 2021a). Thus, the mean contribution of horizontal transport to O<sub>3</sub> mass  
454 in summer was lower than in autumn. Of particular interest is the variation of the contributions of horizontal transport  
455 through the south border of the PRD before and after ~14:00 LT, as indicated by the results of the O<sub>3</sub> mass budget (Fig. 4).  
456 Besides, both O<sub>3</sub> budgets suggest notable O<sub>3</sub> mass and concentration decreases due to ABLex-A in the afternoon. These  
457 phenomena are both related to the influence of sea breezes.

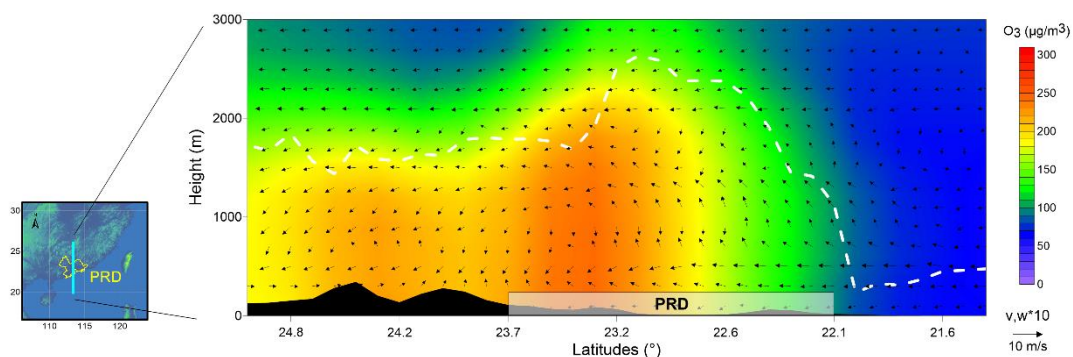
458

459 Figure 5 shows the near-surface wind roses at 14:00, 16:00 and 18:00 LT of O<sub>3</sub> polluted days in July 2016 based on the  
460 observational and modelling results in the national meteorological sites within the PRD. At 14:00 LT, the main wind  
461 directions were W, SW and NW in both datasets. More S and SE winds occurred in later hours, and they became the  
462 prevailing winds at 18:00 LT, suggesting the gradual development of sea breezes in the PRD. Thus, O<sub>3</sub> was originally  
463 transported out of the PRD through the south border with negative contributions to O<sub>3</sub> mass; in the late afternoon, sea  
464 breezes reversed the directions of O<sub>3</sub> transport, resulting in positive contributions to O<sub>3</sub> mass by horizontal transport through  
465 the south border (Fig. 4). Moreover, the development of sea breezes is connected to the changes of wind fields not only  
466 horizontally, but also vertically. Taking the O<sub>3</sub> polluted day July 24th, 2016 for example, the cross-section of O<sub>3</sub>  
467 concentrations and wind fields in the PRD at 16:00 LT of the day is shown in Fig. 6 (the cross-section is made along the  
468 113.2° E longitude, ranging from 26.0° to 20.0° N in latitude). Strong southerly wind and lower O<sub>3</sub> concentrations are found  
469 in the southern PRD, indicating the influence of sea breezes during that time. Near the interfaces where sea breezes  
470 encountered local air parcels (indicated by the drastic increase in O<sub>3</sub> concentrations from less than 100 µg/m<sup>3</sup> to about 100-  
471 150 µg/m<sup>3</sup>), updrafts occurred, suggesting the formation of sea breeze front (Ding et al., 2004; You and Fung, 2019). The  
472 front promoted the upward transport of O<sub>3</sub> from the ABL, or considerable O<sub>3</sub> mass decrease due to ABLex-A. Both  
473 horizontal transport and ABLex-A led to decreased O<sub>3</sub> concentrations, because under the effect of sea breezes, clean air

474 parcels were transported into the region and polluted air parcels were transported out of the region. The influence of sea  
 475 breezes can also be seen in autumn but was weaker and occurred later than in summer. Besides, in autumn, horizontal  
 476 transport through the south border of the PRD contributed to the increase of O<sub>3</sub> concentration at night, indicating the effects  
 477 of O<sub>3</sub> recirculation from the “O<sub>3</sub> pool” in the bay areas to the south of the PRD (Zeren et al., 2019; Zeren et al., 2022).  
 478  
 479 Through the calculations and analyses of transport contributions in the two O<sub>3</sub> budgets, the influences of complex transport  
 480 processes on multiple scales to O<sub>3</sub> concentration and mass can be well identified. These results provide a deeper  
 481 understanding of how transport influences regional O<sub>3</sub> pollution in the PRD.  
 482



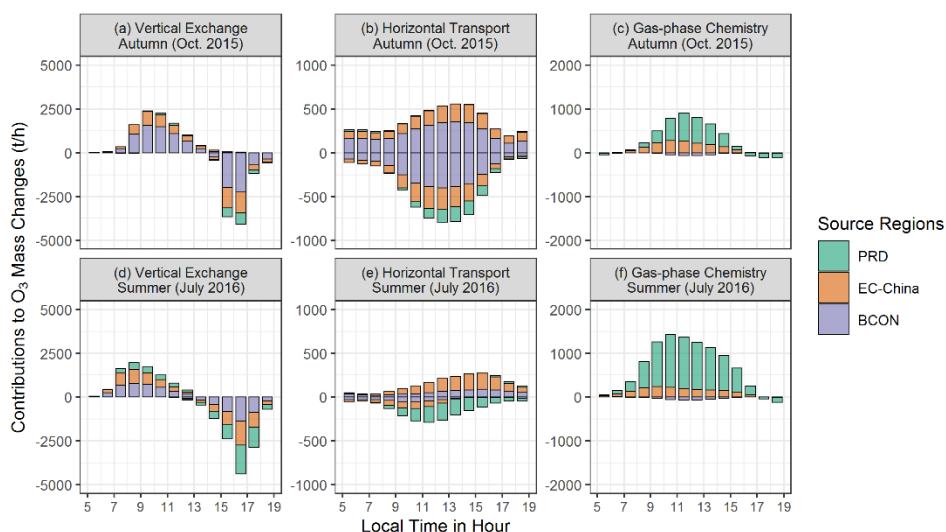
483  
 484 **Figure 5.** Wind roses at 14:00, 16:00, and 18:00 local time (LT) of the O<sub>3</sub> polluted days in July 2016 in the Pearl River Delta (PRD).  
 485 Observational and modelling wind speeds and directions in 29 national meteorological sites within the PRD were used for this figure.



486  
 487 **Figure 6.** Cross-section of O<sub>3</sub> concentrations (µg/m<sup>3</sup>) and wind fields at 16:00 local time on July 24th, 2016. The dashed white line  
 488 indicates the top of the atmospheric boundary layer. PRD, Pearl River Delta.

#### 489 4 Effects of transport and photochemistry on the regional origins of O<sub>3</sub>

490 Based on reported publications (Li et al., 2012; Li et al., 2013; Yang et al., 2019; Gao et al., 2020), O<sub>3</sub> in the PRD is mostly  
491 derived from emissions outside the PRD and background O<sub>3</sub>, rather than local emissions. This is the same for the O<sub>3</sub> polluted  
492 days in the representative months of autumn and summer in this study, when the contributions of non-local sources account  
493 for, on average, 89% and 65% of the O<sub>3</sub> in the PRD, respectively, in 9:00-17:00 LT (55% and 32% contributed by BCON,  
494 34% and 33% contributed by EC-China in the two months; Qu et al., 2021a). To explain why non-local sources are dominant  
495 for O<sub>3</sub> in the PRD, by combining O<sub>3</sub> mass budget calculation with O<sub>3</sub> source apportionment (method introduced in Sect. 2.6),  
496 we identified the regional origins of O<sub>3</sub> mass changes due to vertical exchange through the ABL top, horizontal transport and  
497 gas-phase chemistry (Fig. 7). Here, the contributions of three sources to the O<sub>3</sub> mass increase and decrease were both  
498 quantified. But further analyses focus on the results related to O<sub>3</sub> mass increase, because the origins of O<sub>3</sub> in the region are  
499 more likely to be influenced by the “new O<sub>3</sub>” transported into and produced within the PRD.



500

501 **Figure 7.** The regional origins of hourly O<sub>3</sub> mass changes contributed by (a,d) vertical exchange through the ABL top, (b,e) horizontal  
502 transport, and (c,f) gas-phase chemistry on the polluted days of representative months in autumn (Oct. 2015; a-c) and summer (July 2016;  
503 d-f). The results for the time window 5:00-19:00 LT are shown here. PRD, Pearl River Delta; EC-China, East and Central China; BCON,  
504 the boundary conditions of d02 modelling, or the contribution of sources outside the d02. Note that the scales are different among the three  
505 columns.

506

507 Through vertical exchange through the ABL top, massive non-local O<sub>3</sub> entered into the ABL of the PRD. In the morning-  
508 hour O<sub>3</sub> mass increase due to this process, BCON and EC-China accounted for 65% and 31%, respectively, in autumn. By  
509 contrast, local emissions only contributed 4% to this transported O<sub>3</sub> during the same period, suggesting that local O<sub>3</sub> was less  
510 likely to be recirculated back to the PRD during daytime. In summer, the contribution of local emissions in the O<sub>3</sub> mass  
511 transported into the region through vertical exchange was higher than in autumn, reaching 20% during the morning hours.

512 However, non-local sources still dominated the O<sub>3</sub> mass increase due to vertical exchange — the morning-hour contributions  
513 in percentage of BCON and EC-China were 42% and 38%, respectively.

514

515 O<sub>3</sub> mass increase due to horizontal transport was connected to the contribution of non-local sources as well. In both seasons,  
516 O<sub>3</sub> transported into the PRD originated almost exclusively from EC-China and BCON.

517

518 It is not surprising that most O<sub>3</sub> produced through photochemistry (daytime gas-phase chemistry) was related to local  
519 emissions, of which the contributions accounted for 66% and 82% during the daytime of autumn (6:00-18:00 LT) and  
520 summer (5:00-19:00 LT), respectively. The contributions of EC-China emissions in the daytime O<sub>3</sub> mass increase reached  
521 34% and 18% in the two seasons, respectively, indicating that the influences of non-local O<sub>3</sub> precursor import on local O<sub>3</sub>  
522 photochemistry are also considerable in the PRD.

523

524 With the results of the O<sub>3</sub> mass budget and the regional origins of O<sub>3</sub> mass increase due to transport and photochemistry, the  
525 effect of O<sub>3</sub>-related processes on the origins of O<sub>3</sub> can be revealed. Based on the O<sub>3</sub> mass budget, the accumulated morning-  
526 hour O<sub>3</sub> mass increase exceeded 10000 tons for both seasons, which is 6-9 times larger than the original O<sub>3</sub> mass in the ABL  
527 of the PRD before sunrise (< 1500 tons). Thus, in the daytime, most O<sub>3</sub> in the PRD was the “new O<sub>3</sub>” contributed by  
528 transport and photochemistry, and the origins of O<sub>3</sub> within the region were nearly determined by these of newly transported  
529 and produced O<sub>3</sub>. By combining the O<sub>3</sub> mass budget and O<sub>3</sub> source apportionment, we identified the O<sub>3</sub> mass increase due to  
530 O<sub>3</sub>-related processes as local (PRD) and non-local (EC-China and BCON) contributions. According to the results discussed  
531 before, high contributions of transport in the morning-hour O<sub>3</sub> mass increase and the dominance of non-local source  
532 contributions in this part of new O<sub>3</sub> ensure that non-local sources contributed to most O<sub>3</sub> in the PRD. Moreover, differences  
533 in the contributions of O<sub>3</sub>-related processes in the O<sub>3</sub> mass budget as well as the origins of morning-hour O<sub>3</sub> mass increase  
534 lead to varied origins of O<sub>3</sub> in the region. For instance, when comparing the results of O<sub>3</sub> source apportionment in the two  
535 seasons, we found that the contributions of non-local sources (local emissions) to O<sub>3</sub> were lower (higher) in summer than in  
536 autumn. It can be attributed to the combined effects of increased photochemistry contributions (or decreased transport  
537 contributions) in the O<sub>3</sub> mass increase and reduced non-local source contributions in both transported and chemically  
538 produced O<sub>3</sub> in summer. Collectively, these changes lead to reduced non-local contributions (or higher local contributions) to  
539 O<sub>3</sub>.

540

541 By influencing O<sub>3</sub> mass increase and its regional origins, transport and photochemistry determine the results of O<sub>3</sub> source  
542 apportionment within the region. Specifically, transport (mainly ABLex-H) brings massive non-local O<sub>3</sub> into the region in  
543 the morning, explaining why most O<sub>3</sub> in the PRD is derived from non-local sources. However, accompanied with the  
544 simultaneous rapid increase of ABL volumes, this process has a relatively limited contribution to O<sub>3</sub> concentration increase  
545 in comparison to photochemistry. The O<sub>3</sub> concentration budget only concerns the influence of O<sub>3</sub>-related processes on the

546 variations of O<sub>3</sub> concentration, thus it fails to illustrate the effect of transport on the regional origin of O<sub>3</sub>. Our results  
547 highlight the difference between the O<sub>3</sub> concentration and mass budgets, which may result in distinct understandings about  
548 the role of transport and photochemistry in regional O<sub>3</sub> pollution. To completely illustrate the effects of two O<sub>3</sub>-related  
549 processes on regional O<sub>3</sub> pollution, insights from both O<sub>3</sub> budgets are required.

## 550 **5 Conclusion and outlook**

551 To effectively alleviate O<sub>3</sub> pollution, it is important to understand the respective role of transport and photochemistry in  
552 regional O<sub>3</sub> pollution. The O<sub>3</sub> concentration budget is widely used to quantify the contributions of these O<sub>3</sub>-related processes  
553 to the variations of O<sub>3</sub> concentrations, and it often concludes that photochemistry is the main contributor to the aggravation  
554 of O<sub>3</sub> pollution. However, it does not explain why most of the O<sub>3</sub> is transported from the outside regions as indicated by O<sub>3</sub>  
555 source apportionment studies. To comprehensively illustrate the effects of transport and photochemistry on regional O<sub>3</sub>  
556 pollution, based on the modelling results of WRF-CMAQ, this study presents a method to quantify not only the O<sub>3</sub>  
557 concentration budget, but also the O<sub>3</sub> mass budget, in which the contributions of O<sub>3</sub>-related processes (including transport  
558 and photochemistry) to the variations of mean O<sub>3</sub> concentrations and total O<sub>3</sub> mass within the ABL of the PRD are separately  
559 identified. The different effects of transport on O<sub>3</sub> concentration and mass were considered in the above calculations. The O<sub>3</sub>  
560 concentration budget in the PRD reveals that gas-phase chemistry, including daytime photochemistry and night-time O<sub>3</sub>  
561 titration/depletion, drives the variations of O<sub>3</sub> concentration. Particularly, photochemistry contributed 74% and 95% to the  
562 O<sub>3</sub> concentration increase in the morning hours of autumn and summer months, respectively. In contrast, transport,  
563 especially the vertical exchange through the ABL top, is the main process contributing to the O<sub>3</sub> mass increase in the  
564 morning (78% and 53% in autumn and summer, respectively) and decrease in the afternoon (> 90%). The diurnal changes of  
565 transport contributions in the two O<sub>3</sub> budgets are closely connected to the variations of the ABL and regional wind fields,  
566 including the seasonal prevailing winds and local circulations (sea breezes), in the PRD. Massive O<sub>3</sub>, mostly derived from  
567 non-local sources, being transported into the ABL in the morning has a relatively limited influence on the O<sub>3</sub> concentration  
568 increase (25% and 5% in autumn and summer, respectively) compared to photochemistry because of the rapid change of  
569 ABL volumes at the same time. However, this process nearly determines the dominance of non-local source contributions  
570 for daytime O<sub>3</sub> in the PRD. The two O<sub>3</sub> budgets show notable differences, but together they provide a more complete  
571 overview of the effects of transport and photochemistry on regional O<sub>3</sub> pollution.

572

573 It should be noted that the conclusions in this study apply not only to O<sub>3</sub>, but also to other pollutants with moderately long  
574 atmospheric lifetimes, including fine particulate matter and some of its components. In theory, transport and chemical  
575 transformations are both important processes for these pollutants. However, transport has different effects on the  
576 concentration and mass of pollutants on an hourly scale, which is similar to the discussion in Sect. 2.4. Furthermore, besides  
577 regional origins, the difference between the two budgets may also contribute to the inconsistency of other characteristics of

578 pollutants, such as the contributions of different reaction pathways and sensitivities to precursor emissions, identified by the  
579 concentration budget and mass-based methods. When large quantities of pollutants with different characteristics are  
580 transported into the region, the variation of their concentrations is often not perceptible and thus neglected in the  
581 concentration budget. However, as indicated by this study, the transport processes are likely to change or even determine the  
582 characteristics of pollutants within the region. Therefore, we suggest that attention should be paid to selecting a proper  
583 budget type and using correct budget calculation methods in related research. But to fully reveal the effects of transport,  
584 chemistry and other related processes on regional pollution, insights from both concentration and mass budgets are  
585 necessary.

586

587 Uncertainty remains in the calculated O<sub>3</sub> budgets, which is partly related to the biases in the modelling results. Therefore,  
588 supporting observations are essential for future research. Recent progress in observational techniques (Zhao et al., 2021;  
589 Zhou et al., 2021) has enabled three-dimensional measurements of meteorological parameters and O<sub>3</sub> concentrations with  
590 high spatiotemporal resolution and coverage. These data can be used not only for the model validation of key parameters in  
591 budget calculations, but also for the comparisons between observation- and modelling-based contributions by various O<sub>3</sub>-  
592 related processes in O<sub>3</sub> budgets (Kaser et al., 2017). The comparison of contributions by O<sub>3</sub>-related processes is indicative of  
593 the main uncertainties in O<sub>3</sub> pollution modelling, and is therefore also important for further model developments.

594

595 The present study concluded that transport and gas-phase chemistry play the main role in the O<sub>3</sub> mass and concentration  
596 budgets, respectively. As a consequence of our assessment, the following is suggested for policy-makers. For areas where  
597 non-local emissions notably contribute to O<sub>3</sub>, emission reduction in the upwind regions can reduce the overall O<sub>3</sub>  
598 concentrations effectively, which is a crucial step towards the long-term improvement of regional air quality. However, for  
599 short-term air pollution control, this strategy is not efficient because emission reduction in upwind regions may need to start  
600 days earlier before the polluted periods. In contrast, reducing local emissions is expected to lower the rapid daytime O<sub>3</sub>  
601 concentration increase efficiently and, thereby, O<sub>3</sub> peak levels in the short term, as highlighted by the O<sub>3</sub> concentration  
602 budget. The choice of the better strategy to be applied should depend on the specific objectives of O<sub>3</sub> control (mean levels vs.  
603 peak levels; long-term vs. short-term), which are set based on a more in-depth understanding of O<sub>3</sub> effects on human health,  
604 crop yields and ecosystems. More efforts are required to systematically evaluate the effects of different emission reduction  
605 strategies on alleviating the detrimental effects of O<sub>3</sub>.

606

607 *Data availability.* The source codes of WRF and CMAQ are available at the site  
608 [https://www2.mmm.ucar.edu/wrf/users/download/get\\_sources.html](https://www2.mmm.ucar.edu/wrf/users/download/get_sources.html) and <https://www.cmascenter.org/cmaq/>, respectively.  
609 FNL meteorological input files were downloaded from the site <https://rda.ucar.edu/datasets/ds083.2/>. MEIC v1.3  
610 anthropogenic emission inventory is available at [http://meicmodel.org/?page\\_id=560](http://meicmodel.org/?page_id=560). The source codes of MEGAN can be  
611 found at <https://bai.ess.uci.edu/megan/data-and-code>. IAGOS dataset used in model validation was searched and downloaded

612 from <http://iagos-data.fr>, which includes all profiles measured in flights taking off from and landing in Hong Kong during  
613 the two representative months. We also provided the initial Fortran code used in ozone budget calculations and hourly O<sub>3</sub>  
614 concentration and mass budget results in the two representative months (the initial data of Fig. 4) at  
615 <https://doi.org/10.5281/zenodo.6259253>.

616

617 *Author contributions.* KQ, XW and YZ designed the study. KQ, XW, TX did the simulations using the WRF-CMAQ model.  
618 JS, LZ and YZ provided observational results for model validation. KQ, XW, XC, YY, XJ and YZ developed the post-  
619 processing tool *flux\_4d\_cal*, conducted and analysed O<sub>3</sub> budget results. KQ, XW, MV, MK, GB and YZ wrote and/or revised  
620 this paper, with critical feedbacks from all other authors.

621

622 *Competing interests.* One of the authors is a member of the editorial board of Atmospheric Chemistry and Physics, and the  
623 peer-review process was guided by an independent editor. The authors declare no other conflict of interest.

624

625 *Acknowledgements.* This study was supported by the National Key Research and Development Program of China (grant No.  
626 2018YFC0213204), the National Science and Technology Pillar Program of China (grant No. 2014BAC21B01) and the co-  
627 funded DFG-NSFC Sino-German AirChanges project (grant No. 448720203).

628

629 **References**

- 630 Ainsworth, E. A.: Understanding and improving global crop response to ozone pollution, *Plant J.*, 90, 886–897,  
631 <https://doi.org/10.1111/tpj.13298>, 2017.
- 632 Bates, K. H. and Jacob, D. J.: An expanded definition of the odd oxygen family for tropospheric ozone budgets: Implications  
633 for ozone lifetime and stratospheric influence, *Geophys. Res. Lett.*, 47, e2019GL084486,  
634 <https://doi.org/10.1029/2019GL084486>, 2019.
- 635 Boian, C. and Andrade, M. D. F.: Characterization of ozone transport among metropolitan regions, *Rev. Bras. Meteorol.*, 27,  
636 229–242, <https://doi.org/10.1590/S0102-77862012000200009>, 2012.
- 637 Carter, W. P. L.: Development of the SAPRC-07 chemical mechanism, *Atmos. Environ.*, 44, 5324–5335,  
638 <https://doi.org/10.1016/j.atmosenv.2010.01.026>, 2010.
- 639 Chang, X., Wang, S., Zhao, B., Cai, S., and Hao, J.: Assessment of inter-city transport of particulate matter in the Beijing–  
640 Tianjin–Hebei region, *Atmos. Chem. Phys.*, 18, 4843–4858, <https://doi.org/10.5194/acp-18-4843-2018>, 2018.
- 641 Clappier, A., Belis, C. A., Pernigotti, D., and Thunis, P.: Source apportionment and sensitivity analysis: two methodologies  
642 with two different purposes, *Geosci. Model Dev.*, 10, 4245–4256, <https://doi.org/10.5194/gmd-10-4245-2017>, 2017.
- 643 Ding, A., Wang, T., Zhao, M., Wang, T. J., and Li, Z. K.: Simulation of sea-land breezes and a discussion of their  
644 implications on the transport of air pollution during a multi-day ozone episode in the Pearl River Delta of China,  
645 *Atmos. Environ.*, 38, 6737–6750, <https://doi.org/10.1016/j.atmosenv.2004.09.017>, 2004.
- 646 Fishman, J., Wozniak, A. E., and Creilson, J. K.: Global distribution of tropospheric ozone from satellite measurements  
647 using the empirically corrected tropospheric ozone residual technique: Identification of the regional aspects of air  
648 pollution, *Atmos. Chem. Phys.*, 3, 893–907, <https://doi.org/10.5194/acp-3-893-2003>, 2003.
- 649 Fleming, Z. L., Doherty, R. M., von Schneidmesser, E., Malley, C. S., Cooper, O. R., Pinto, J. P., Colette, A., Xu, X. B.,  
650 Simpson, D., Schultz, M. G., Lefohn, A. S., Hamad, S., Moolla, R., Solberg, S., and Feng, Z. Z.: Tropospheric ozone  
651 assessment report: Present-day ozone distribution and trends relevant to human health, *Elementa-Sci. Anthropol.*, 6, 12,  
652 <https://doi.org/10.1525/elementa.273>, 2018.
- 653 Fowler, D., Brimblecombe, P., Burrows, J., Heal, M. R., Grennfelt, P., Stevenson, D. S., Jowett, A., Nemitz, E., Coyle, M.,  
654 Liu, X., Chang, Y., Fuller, G. W., Sutton, M. A., Klimont, Z., Unsworth, M. H., and Vieno, M.: A chronology of global  
655 air quality, *Philos. T. R. Soc. A*, 378, 20190314, <https://doi.org/10.1098/rsta.2019.0314>, 2020.
- 656 Gao, M., Gao, J., Zhu, B., Kumar, R., Lu, X., Song, S., Zhang, Y., Jia, B., Wang, P., Beig, G., Hu, J., Ying, Q., Zhang, H.,  
657 Sherman, P., and McElroy, M. B.: Ozone pollution over China and India: seasonality and sources, *Atmos. Chem. Phys.*,  
658 20, 4399–4414, <https://doi.org/10.5194/acp-20-4399-2020>, 2020.
- 659 Gao, X., Deng, X., Tan, H., Wang, C., Wang, N., and Yue, D.: Characteristics and analysis on regional pollution process and  
660 circulation weather types over Guangdong Province, *Acta Scientiae Circumstantiae (in Chinese)*, 38(5), 1708–1716,  
661 <https://doi.org/10.13671/j.hjkxxb.2017.0473>, 2018.



662 Guo, J. J., Fiore, A. M., Murray, L. T., Jaffe, D. A., Schnell, J. L., Moore, C. T., and Milly, G. P.: Average versus high  
663 surface ozone levels over the continental USA: model bias, background influences, and interannual variability, *Atmos.*  
664 *Chem. Phys.*, 18, 12123–12140, <https://doi.org/10.5194/acp-18-12123-2018>, 2018.

665 He, K.: Multi-resolution Emission Inventory for China (MEIC): model framework and 1990-2010 anthropogenic emissions,  
666 American Geophysical Union, Fall Meeting 2012, 3–7 December 2012, San Francisco, USA, A32B-05, 2012.

667 Hou, X., Zhu, B., Kang, H., and Gao, J.: Analysis of seasonal ozone budget and spring ozone latitudinal gradient variation in  
668 the boundary layer of the Asia-Pacific region, *Atmos. Environ.*, 94, 734–741,  
669 <https://doi.org/10.1016/j.atmosenv.2014.06.006>, 2014.

670 Hu, J., Li, Y., Zhao, T., Liu, J., Hu, X.-M., Liu, D., Jiang, Y., Xu, J., and Chang, L.: An important mechanism of regional O<sub>3</sub>  
671 transport for summer smog over the Yangtze River Delta in eastern China, *Atmos. Chem. Phys.*, 18, 16239–16251,  
672 <https://doi.org/10.5194/acp-18-16239-2018>, 2018.

673 Janssen, R. H. H. and Pozzer, A.: Description and implementation of a MiXed Layer model (MXL, v1.0) for the dynamics of  
674 the atmospheric boundary layer in the Modular Earth Submodel System (MESSy), *Geosci. Model Dev.*, 8, 453–471,  
675 <https://doi.org/10.5194/gmd-8-453-2015>, 2015.

676 Jin, X., Cai, X., Huang, Q., Wang, X., Song, Y., and Zhu, T.: Atmospheric boundary layer—free troposphere air exchange in  
677 the North China Plain and its impact on PM<sub>2.5</sub> pollution, *J. Geophys. Res.-Atmos.*, 126(9), e2021JD034641,  
678 <https://doi.org/10.1029/2021JD034641>, 2021.

679 Kaser, L., Patton, E. G., Pfister, G. G., Weinheimer, A. J., Montzka, D. D., Flocke, F., Thompson, A. M., Stauffer, R. M.,  
680 and Halliday, H. S.: The effect of entrainment through atmospheric boundary layer growth on observed and modeled  
681 surface ozone in the Colorado Front Range, *J. Geophys. Res.-Atmos.*, 122, 6075–6093,  
682 <https://doi.org/10.1002/2016JD026245>, 2017.

683 Laughner, J. L. and Cohen, R. C.: Direct observation of changing NO<sub>x</sub> lifetime in North American cities, *Science*, 366, 723–  
684 727, <https://doi.org/10.1126/science.aax6832>, 2019.

685 Lee, X.: *Fundamentals of Boundary-Layer Meteorology*, Springer Atmospheric Sciences., 2018.

686 Lelieveld, J., Hoor, P., Jöckel, P., Pozzer, A., Hadjinicolaou, P., Cammas, J.-P., and Beirle, S.: Severe ozone air pollution in  
687 the Persian Gulf region, *Atmos. Chem. Phys.*, 9, 1393–1406, <https://doi.org/10.5194/acp-9-1393-2009>, 2009.

688 Lenschow, D. H., Pearson, R., and Stankov, B. B.: Estimating the ozone budget in the boundary layer by use of aircraft  
689 measurements of ozone eddy flux and mean concentration, *J. Geophys. Res.*, 86, 7291–7297,  
690 <https://doi.org/10.1029/JC086iC08p07291>, 1981.

691 Li, L., Xie, F., Li, J., Gong, K., Xie, X., Qin, Y., Qin, M., and Hu, J.: Diagnostic analysis of regional ozone pollution in  
692 Yangtze River Delta, China: A case study in summer 2020, *Sci. Total Environ.*, 812, 151511,  
693 <https://doi.org/10.1016/j.scitotenv.2021.151511>, 2021.

694 Li, M., Zhang, Q., Kurokawa, J.-I., Woo, J.-H., He, K., Lu, Z., Ohara, T., Song, Y., Streets, D. G., Carmichael, G. R., Cheng,  
695 Y., Hong, C., Huo, H., Jiang, X., Kang, S., Liu, F., Su, H., and Zheng, B.: MIX: a mosaic Asian anthropogenic emission

696 inventory under the international collaboration framework of the MICS-Asia and HTAP, *Atmos. Chem. Phys.*, 17, 935–  
697 963, <https://doi.org/10.5194/acp-17-935-2017>, 2017.

698 Li, Y., Lau, A. K. H., Fung, J. C. H., Ma, H., and Tse, Y.: Systematic evaluation of ozone control policies using an Ozone  
699 Source Apportionment method, *Atmos. Environ.*, 76, 136–146, <https://doi.org/10.1016/j.atmosenv.2013.02.033>, 2013.

700 Li, Y., Lau, A. K. H., Fung, J. C. H., Zheng, J. Y., Zhong, L. J., and Louie, P. K. K.: Ozone source apportionment (OSAT) to  
701 differentiate local regional and super-regional source contributions in the Pearl River Delta region, China, *J. Geophys.*  
702 *Res.-Atmos.*, 117, D15305, <http://doi.org/10.1029/2011JD017340>, 2012.

703 Liu, F., Beirle, S., Zhang, Q., Dörner, S., He, K., and Wagner, T.: NO<sub>x</sub> lifetimes and emissions of cities and power plants in  
704 polluted background estimated by satellite observations, *Atmos. Chem. Phys.*, 16, 5283–5298,  
705 <https://doi.org/10.5194/acp-16-5283-2016>, 2016.

706 Liu, H. L., Zhang, M. G., and Han, X.: A review of surface ozone source apportionment in China, *Atmos. Ocean. Sci. Lett.*,  
707 13, 470–484, <https://doi.org/10.1080/16742834.2020.1768025>, 2020.

708 Liu, P., Zhang, Y., Yu, S. C., and Schere, K. L.: Use of a Process Analysis tool for diagnostic study on fine particulate matter  
709 predictions in the U.S. Part II: Process Analysis and sensitivity simulations, *Atmos. Pollut. Res.*, 2, 61–71,  
710 <https://doi.org/10.5094/APR.2011.008>, 2011.

711 Massagué, J., Carnerero, C., Escudero, M., Baldasano, J. M., Alastuey, A., and Querol, X.: 2005–2017 ozone trends and  
712 potential benefits of local measures as deduced from air quality measurements in the north of the Barcelona  
713 metropolitan area, *Atmos. Chem. Phys.*, 19, 7445–7465, <https://doi.org/10.5194/acp-19-7445-2019>, 2019.

714 Mills, G., Wagg, S., and Harmens, H.: Ozone pollution: impacts on ecosystem services and biodiversity (CEH Project no.  
715 C04062, C04325), Bangor, UK, NERC/Centre for Ecology & Hydrology, 2013.

716 Myriokefalitakis, S., Daskalakis, N., Fanourgakis, G. S., Voulgarakis, A., Krol, M. C., de Brugh, J. A., and Kanakidou, M.:  
717 Ozone and carbon monoxide budgets over the Eastern Mediterranean, *Sci. Total Environ.*, 563, 40–52,  
718 <https://doi.org/10.1016/j.scitotenv.2016.04.061>, 2016.

719 Naik, V., Szopa, S., Adhikary, B., Artaxo, P., Berntsen, T., Collins, W. D., Fuzzi, S., Gallardo, L., Kiendler Scharr, A.,  
720 Klimont, Z., Liao, H., Unger, N., and Zanis, P.: Short-Lived Climate Forcers, in: *Climate Change 2021: The Physical*  
721 *Science Basis. Contribution of Working Group I to the Sixth Assessment Report of the Intergovernmental Panel on*  
722 *Climate Change*, edited by: Masson-Delmotte, V., Zhai, P., Pirani, A., Connors, S. L., Péan, C., Berger, S., Caud, N.,  
723 Chen, Y., Goldfarb, L., Gomis, M. I., Huang, M., Leitzell, K., Lonnoy, E., Matthews, J. B. R., Maycock, T. K.,  
724 Waterfield, T., Yelekçi, O., Yu, R., and Zhou, B., Cambridge University Press, Cambridge, United Kingdom and New  
725 York, NY, USA, 817–922, <https://doi.org/10.1017/9781009157896.008>, 2021.

726 Novel, D. P.: The OTC challenge: Adding VOC controls in the northeast, *J. Air Waste Manag. Assoc.*, 42(8), 1053–1056,  
727 <https://doi.org/10.1080/10473289.1992.10467050>, 1992.

728 Pay, M. T., Gangoiiti, G., Guevara, M., Napelenok, S., Querol, X., Jorba, O., and Pérez García-Pando, C.: Ozone source  
729 apportionment during peak summer events over southwestern Europe, *Atmos. Chem. Phys.*, 19, 5467–5494,  
730 <https://doi.org/10.5194/acp-19-5467-2019>, 2019.

731 Petzold, A., Thouret, V., Gerbig, C., Zahn, A., Brenninkmeijer, C. A. M., Gallagher, M., Hermann, M., Pontaud, M., Ziereis,  
732 H., Boulanger, D., Marshall, J., Nédélec, P., Smit, H. G. J., Friess, U., Flaud, J.-M., Wahner, A., Cammas, J.-P., Volz-  
733 Thomas, A. and IAGOS TEAM: Global-scale atmosphere monitoring by in-service aircraft—current achievements and  
734 future prospects of the European Research Infrastructure IAGOS, *Tellus B*, 67, 28452,  
735 <https://doi.org/10.3402/tellusb.v67.28452>, 2015.

736 Qu, K., Wang, X., Xiao, T., Shen, J., Lin, T., Chen, D., He, L., Huang, X., Zeng, L., Lu, K., Ou, Y., and Zhang, Y.: Cross-  
737 regional transport of PM<sub>2.5</sub> nitrate in the Pearl River Delta, China: Contributions and mechanisms, *Sci. Total Environ.*,  
738 753, 142439, <https://doi.org/10.1016/j.scitotenv.2020.142439>, 2021b.

739 Qu, K., Wang, X., Yan, Y., Shen, J., Xiao, T., Dong, H., Zeng, L., and Zhang, Y.: A comparative study to reveal the  
740 influence of typhoons on the transport, production and accumulation of O<sub>3</sub> in the Pearl River Delta, China, *Atmos.*  
741 *Chem. Phys.*, 21, 11593–11612, <https://doi.org/10.5194/acp-21-11593-2021>, 2021a.

742 Reid, N., Yap, D., and Bloxam, R.: The potential role of background ozone on current and emerging air issues: An overview,  
743 *Air Qual. Atmos. Health*, 1, 19–29, <https://doi.org/10.1007/s11869-008-0005-z>, 2008.

744 Schultz, M. G., Schröder, S., Lyapina, O., Cooper, O., Galbally, I., Petropavlovskikh, I., Von Schneidmesser, E., Tanimoto,  
745 H., Elshorbany, Y., Naja, M., Seguel, R., Dauert, U., Eckhardt, P., Feigenspahn, S., Fiebig, M., Hjellbrekke, A.-G.,  
746 Hong, Y.-D., Kjeld, P. C., Koide, H., Lear, G., Tarasick, D., Ueno, M., Wallasch, M., Baumgardner, D., Chuang, M.-T.,  
747 Gillett, R., Lee, M., Molloy, S., Moolla, R., Wang, T., Sharps, K., Adame, J. A., Ancellet, G., Apadula, F., Artaxo, P.,  
748 Barlasina, M., Bogucka, M., Bonasoni, P., Chang, L., Colomb, A., Cuevas, E., Cupeiro, M., Degorska, A., Ding, A.,  
749 Fröhlich, M., Frolova, M., Gadhavi, H., Gheusi, F., Gilge, S., Gonzalez, M. Y., Gros, V., Hamad, S. H., Helmig, D.,  
750 Henriques, D., Hermansen, O., Holla, R., Huber, J., Im, U., Jaffe, D. A., Komala, N., Kubistin, D., Lam, K.-S., Laurila,  
751 T., Lee, H., Levy, I., Mazzoleni, C., Mazzoleni, L., McClure-Begley, A., Mohamad, M., Murovic, M., Navarro-Comas,  
752 M., Nicodim, F., Parrish, D., Read, K. A., Reid, N., Ries, L., Saxena, P., Schwab, J. J., Scorgie, Y., Senik, I.,  
753 Simmonds, P., Sinha, V., Skorokhod, A., Spain, G., Spangl, W., Spoor, R., Springston, S. R., Steer, K., Steinbacher, M.,  
754 Suharguniyawan, E., Torre, P., Trickl, T., Weili, L., Weller, R., Xu, X., Xue, L., and Zhiqiang, M.: Tropospheric ozone  
755 assessment report: Database and metrics data of global surface ozone observations, *Elementa-Sci. Anthropol.*, 5, 58,  
756 <https://doi.org/10.1525/elementa.244>, 2017.

757 Seinfeld, J. H. and Pandis, S. N.: *Atmospheric chemistry and physics: from air pollution to climate change*, John Wiley &  
758 Sons, 2016.

759 Sinclair, V. A., Belcher, S. E., and Gray, S. L.: Synoptic controls on boundary-layer characteristics, *Bound.-Layer Meteorol.*,  
760 134, 387–409, <https://doi.org/10.1007/s10546-009-9455-6>, 2010.

761 Sitch, S., Cox, P. M., Collins, W. J., and Huntingford, C.: Indirect radiative forcing of climate change through ozone effects  
762 on the land-carbon sink, *Nature*, 448, 791–795, <https://doi.org/10.1038/nature06059>, 2007.

763 Stevenson, D. S., Dentener, F. J., Schultz, M. G., Ellingsen, K., van Noije, T. P. C., Wild, O., Zeng, G., Amann, M.,  
764 Atherton, C. S., Bell, N., Bergmann, D. J., Bey, I., Butler, T., Cofala, J., Collins, W. J., Derwent, R. G., Doherty, R. M.,  
765 Drevet, J., Eskes, H. J., Fiore, A. M., Gauss, M., Hauglustaine, D. A., Horowitz, L. W., Isaksen, I. S. A., Krol, M. C.,  
766 Lamarque, J.-F., Lawrence, M. G., Montanaro, V., Müller, J.-F., Pitari, G., Prather, M. J., Pyle, J. A., Rast, S.,  
767 Rodriguez, J. M., Sanderson, M. G., Savage, N. H., Shindell, D. T., Strahan, S. E., Sudo, K., and Szopa, S.: Multimodel  
768 ensemble simulations of present-day and near-future tropospheric ozone, *J. Geophys. Res.*, 111, D08301,  
769 <https://doi.org/10.1029/2005JD006338>, 2006.

770 Su, R., Lu, K. D., Yu, J. Y., Tan, Z. F., Jiang, M. Q., Li, J., Xie, S. D., Wu, Y. S., Zeng, L. M., Zhai, C. Z., and Zhang, Y. H.:  
771 Exploration of the formation mechanism and source attribution of ambient ozone in Chongqing with an observation-  
772 based model, *Sci. China Earth Sci.*, 61, 23–32, <https://doi.org/10.1007/s11430-017-9104-9>, 2018.

773 Tan, Z., Lu, K., Jiang, M., Su, R., Dong, H., Zeng, L., Xie, S., Tan, Q., and Zhang, Y.: Exploring ozone pollution in  
774 Chengdu, southwestern China: A case study from radical chemistry to O<sub>3</sub>-VOC-NO<sub>x</sub> sensitivity, *Sci. Total Environ.*,  
775 636, 775–786, <https://doi.org/10.1016/j.scitotenv.2018.04.286>, 2018.

776 Tan, Z., Lu, K., Jiang, M., Su, R., Wang, H., Lou, S., Fu, Q., Zhai, C., Tan, Q., Yue, D., Chen, D., Wang, Z., Xie, S., Zeng,  
777 L., and Zhang, Y.: Daytime atmospheric oxidation capacity in four Chinese megacities during the photochemically  
778 polluted season: a case study based on box model simulation, *Atmos. Chem. Phys.*, 19, 3493–3513,  
779 <https://doi.org/10.5194/acp-19-3493-2019>, 2019.

780 Thunis, P., Clappier, A., Tarrason, L., Cuvelier, C., Monteiro, A., Pisoni, E., Wesseling, J., Belis, C. A., Pirovano, G.,  
781 Janssen, S., Guerreiro, C., and Peduzzi, E.: Source apportionment to support air quality planning: Strengths and  
782 weaknesses of existing approaches, *Environ. Int.*, 130, 104825, <https://doi.org/10.1016/j.envint.2019.05.019>, 2019.

783 Trousdell, J. F., Caputi, D., Smoot, J., Conley, S. A., and Faloona, I. C.: Photochemical production of ozone and emissions  
784 of NO<sub>x</sub> and CH<sub>4</sub> in the San Joaquin Valley, *Atmos. Chem. Phys.*, 19, 10697–10716, <https://doi.org/10.5194/acp-19-10697-2019>, 2019.

786 Trousdell, J. F., Conley, S. A., Post, A., and Faloona, I. C.: Observing entrainment mixing, photochemical ozone production,  
787 and regional methane emissions by aircraft using a simple mixed-layer framework, *Atmos. Chem. Phys.*, 16, 15433–  
788 15450, <https://doi.org/10.5194/acp-16-15433-2016>, 2016.

789 Vilà-Guerau De Arellano, J., van Heerwaarden, C. C., van Stratum, B. J. H., and van den Dries, K.: *Atmospheric Boundary  
790 Layer: Integrating Air Chemistry and Land Interactions*, Cambridge University Press, New York, 2015.

791 Yan, F., Gao, Y., Ma, M., Liu, C., Ji, X., Zhao, F., Yao, X., and Gao, H.: Revealing the modulation of boundary conditions  
792 and governing processes on ozone formation over northern China in June 2017, *Environ. Pollut.*, 272, 115999,  
793 <https://doi.org/10.1016/j.envpol.2020.115999>, 2021.

794 Yang, L., Wang, X., and Chen, Q.: New method for investigating regional interactions of air pollutants (in Chinese), *Acta*  
795 *Sci. Circumstantiae*, 32(3), 528-536, <https://doi.org/10.13671/j.hjkxxb.2012.03.012>, 2012.

796 Yang, W., Chen, H., Wang, W., Wu, J., Li, J., Wang, Z., Zheng, J., and Chen, D.: Modeling study of ozone source  
797 apportionment over the Pearl River Delta in 2015, *Environ. Pollut.*, 253, 393-402,  
798 <https://doi.org/10.1016/j.envpol.2019.06.091>, 2019.

799 You, C., and Fung, J. C. H.: Characteristics of the sea-breeze circulation in the Pearl River Delta region and its dynamical  
800 diagnosis. *Journal of Applied Meteorology and Climatology*, 58(4), 741-755, <https://doi.org/10.1175/JAMC-D-18->  
801 0153.1, 2019.

802 Yu, D., Tan, Z., Lu, K., Ma, X., Li, X., Chen, S., Zhu, B., Lin, L., Li, Y., Qiu, P., Yang, X., Liu, Y., Wang, H., He, L.,  
803 Huang, X., and Zhang, Y.: An explicit study of local ozone budget and NO<sub>x</sub>-VOCs sensitivity in Shenzhen China,  
804 *Atmos. Environ.*, 224, 117304, <https://doi.org/10.1016/j.atmosenv.2020.117304>, 2020.

805 Zeren, Y., Guo, H., Lyu, X., Jiang, F., Wang, Y., Liu, X., Zeng, L., Li, M., and Li, L.: An Ozone “Pool” in South China:  
806 Investigations on Atmospheric Dynamics and Photochemical Processes Over the Pearl River Estuary, *J. Geophys. Res.*,  
807 124, 12340–12355, <https://doi.org/10.1029/2019jd030833>, 2019.

808 Zeren, Y., Zhou, B., Zheng, Y., Jiang, F., Lyu, X., Xue, L., Wang, H., Liu, X., and Guo, H.: Does Ozone Pollution Share the  
809 Same Formation Mechanisms in the Bay Areas of China?, *Environ. Sci. Tech.*, 56(20), 14326-14337,  
810 <https://doi.org/10.1021/acs.est.2c05126>, 2022.

811 Zhang, J. J., Wei, Y., and Fang, Z.: Ozone pollution: A major health hazard worldwide, *Front. Immunol.*, 10, 2518,  
812 <https://doi.org/10.3389/fimmu.2019.02518>, 2019.

813 Zhao, R., Hu, Q., Sun, Z., Wu, Y., Xing, C., Liu, H., and Liu, C.: Review of space and ground integrated remote sensing for  
814 air pollutants (in Chinese). *Res. Environ. Sci.*, 34(1), 28-40. <https://doi.org/10.13198/j.issn.1001-6929.2020.11.25>,  
815 2021.

816 Zhao, W., Tang, G., Yu, H., Yang, Y., Wang, Y., Wang, L., An, J., Gao, W., Hu, B., Cheng, M., An, X., Li, X., and Wang,  
817 Y.: Evolution of boundary layer ozone in Shijiazhuang, a suburban site on the North China Plain, *J. Environ. Sci.*, 83,  
818 152–160, <https://doi.org/10.1016/j.jes.2019.02.016>, 2019.

819 Zhou, B., Zhang, S., Xue, R., Li, J., and Wang, S.: A review of Space-Air-Ground integrated remote sensing techniques for  
820 atmospheric monitoring, *J. Environ. Sci.*, <https://doi.org/10.1016/j.jes.2021.12.008>, 2021.

821